Journal of Structural Geology 158 (2022) 104573

Contents lists available at ScienceDirect

Journal of Structural Geology

journal homepage: www.elsevier.com/locate/jsg

The Patos-Pernambuco shear system of NE Brazil: Partitioned intracontinental transcurrent deformation revealed by enhanced aeromagnetic data

Haakon Fossen [a,*], Lyal B. Harris [b], Carolina Cavalcante [c], Carlos José Archanjo [d], Carlos F. Ávila [d]

[a] Museum of Natural History/Department of Earth Science, University of Bergen, Allégaten 41, 5007, Bergen, Norway
[b] INRS-ETE, 490 de la Couronne, Québec, QC, G1K 9A9, Canada
[c] Departamento de Geologia, Universidade Federal do Paraná, Av. Cel. Francisco Heráclito dos Santos, 100, Centro Politécnico, Curitiba, PR, 81531-980, Brazil
[d] Instituto de Geociências, Universidade de São Paulo, São Paulo, SP, Brazil

ARTICLE INFO

Keywords:
Patos and Pernambuco shear zones
Transcurrent intracontinental shear
Brasiliano orogeny
Enhanced aeromagnetics
Ductile shear fabrics

ABSTRACT

The Neoproterozoic-Cambrian (Brasiliano) intracontinental Patos-Pernambuco shear system is developed in Archean to Neoproterozoic crust, reactivating rift margins N of the São Francisco Craton. We here use enhanced aeromagnetic images to reveal internal details of the broad E-W dextral Patos and Pernambuco shear zones, the intervening Central (Transversal) Domain and the adjacent Northern Domain. We estimate shear strains up to 50–60 and a total of ca. 350 and 200 km dextral displacement for the Patos and Pernambuco shear zones, respectively. Deflection of foliations, fold axial surfaces and plutons as well as internal S-C fabrics and asymmetric folds within these large shear zones confirm dextral displacement. However, the dominant population of NE-trending shear zones in the Central Domain, by many considered dextral, are here confirmed to be sinistral and thereby elongating this domain. The Northern Domain behaved differently, hence large-scale Ediacaran strain partitioning in the region is suggested, where different blocks experienced different deformation between major simple-shear dominated shear zones. We show how much more structural information can now be obtained from enhanced aeromagnetic data than from field mapping alone; aeromagnetic interpretations, nevertheless, still draw on analysis techniques epitomized by John Ramsay.

1. Introduction

A rigorous and mathematical definition of a shear zone was presented and explored by Ramsay (1967, 1980), Ramsay and Graham (1970) and Ramsay and Huber (1983). They considered an idealized case of simple shear with or without additional dilation/compaction across the zone. Ramsay's analysis formed the basis for a new way to deal with shear zones and the relation between their displacement, strain and internal structure in a quantitative way, as exposed in several analytical papers from the 1970s and 80s (e.g., Ramsay and Graham, 1970; Ramsay and Allison, 1979; Simpson, 1983). This fundamental framework was soon expanded into more general strain types (Coward, 1976; Coward and Kim, 1981), including sub-simple shear (Ramberg, 1975; Ramberg and Ghosh, 1977; Simpson and De Paor, 1993) and transpression/transtension (Sanderson and Marchini, 1984; Fossen and Tikoff, 1993, 1998; Robin and Cruden, 1994). Another important step forward was the general awareness that deformation in shear zones is not only heterogeneous, but also partitioned into different components, from the grain scale to that of plate boundaries (Lister and Williams, 1983; Tikoff and Teyssier, 1994; Jones and Tanner, 1995; Clegg and Holdsworth, 2005; Carreras et al., 2013) and that many if not most geologic structures repeat themselves at all such scales. Some of the earliest studies of foliation trajectories associated with ductile shear zones were made by John Ramsay (e.g., Ramsay, 1967; Ramsay and Graham, 1970). An excellent understanding of what was later called S-C fabrics, asymmetric boudins, and lineations and folding associated with shear zones followed (e.g., Escher et al., 1975), leading to the classification of shear-related foliations as S-C-C′ structures (e.g., Berthé et al.,

* Corresponding author. Museum of Natural History/Department of Earth Science, University of Bergen, Allégaten 41, 5007, Bergen, Norway.
E-mail addresses: haakon.fossen@uib.no (H. Fossen), lyal.harris@inrs.ca (L.B. Harris), geanecarol@gmail.com (C. Cavalcante), archan@usp.br (C.J. Archanjo), carlosavila@usp.br (C.F. Ávila).

https://doi.org/10.1016/j.jsg.2022.104573
Received 31 October 2021; Received in revised form 28 February 2022; Accepted 12 March 2022
Available online 17 March 2022

1979; Lister and Snoke, 1984) and the frequently observed partitioning of deformation into simple shear bands separating domains dominated by rotation and/or flattening (Dennis and Secor, 1990), and into zones of coaxial deformation within a simple shear zone due to slip along layer contacts (Harris and Cobbold, 1984).

A related example is deformation partitioning in rocks with rigid inclusions such as porphyroclast systems, and understanding the underlying processes enables us to use the resulting asymmetric geometries as kinematic indicators in shear zones (Passchier and Simpson, 1986); they can sometimes also be used to estimate vorticity quantitatively (Marques et al., 2007; Johnson et al., 2009; Ávila et al., 2019). The understanding of S-C-C' structures, and asymmetric shear zone fabrics and other kinematic indicators in general, led in the 1980s to what is arguably the most important advance in field-related structural geology for many decades, allowing kinematics to be readily interpreted from mere field and thin section observations of sheared rock. The same kinematic indicators have subsequently been applied to interpretations of regional ductile shear zones using remote sensing (e.g., Martelat et al., 2000) and aeromagnetic data (Stewart and Betts, 2010; Jessell et al., 2012; Harris and Bédard, 2014; Cleven et al., 2020; Harris, this volume), including mapping strain partitioning in regional transpressional shear systems (e.g., Cleven et al., 2020, their Fig. 16).

Understanding shear zone structures is extremely important, given their close link to tectonics (displacements, strains and kinematics recorded in sheared rocks are paramount to both the identification and testing of regional tectonic models), their controls on mineralization and related hydrothermal fluid flow and pluton emplacement.

In this contribution we will analyze structural aspects of the shear zone network in the Borborema Province in NE Brazil, based on the fundamental knowledge that developed from John Ramsay and others' work in the second half of the 20th century. The shear zone network in the Borborema Province in NE Brazil on the N margin of the São Francisco Craton (Fig. 1), and its extension into Africa on the N margin of the Congo Craton in continental reconstructions (e.g., Caby, 1989; Arthaud et al., 2008) is one of the largest ductile shear zone systems on Earth and covers aspects of shear zone structure from the micro-scale to that of more than 2000 km. In NE Brazil, the shear zone system is reasonably well exposed, mapped on a regional scale by the Brazilian Geological Survey (CPRM, geosgb.cprm.gov.br; Fig. 2a) and, for the most part, covered by a consistent medium-resolution aeromagnetic data set that we here employ to better interpret its internal structure and kinematics. Whilst, with some exceptions (e.g., the combined aeromagnetic and gravity research of Oliveira and Medeiros, 2018 and the study of dikes by Melo et al., 2022), most previous interpretations of aeromagnetic data in the Borborema Province are either detailed local studies (e.g., Santos et al., 2017; Pereira et al., 2019) or were applied more to mapping of lithostratigraphy, igneous intrusions, and basement fabric controls on rifts (Bezerra et al., 2014; Vasconcelos et al., 2019), and not the detailed structure of the Brasiliano shear network. Mocitaiba et al. (2017) present low resolution aeromagnetic images for the Parnaíba Basin overlying the western part of this shear system, though only an approximation of the continuation of the two main E-W shears is discernible (flight lines are mainly from 1 to 4 km apart, although one small area is covered by 500 m line data). Our focus, however, is to use enhanced aeromagnetic data to study the kinematics and geometry of structures of the two major Patos and Pernambuco shear zones of the region and the E-W trending deformed Central Domain (a.k.a. Transversal Domain; Van Schmus et al., 2011), and in part the Northern Domain adjacent to the Patos shear zone. A subordinate aim is to show how different enhancements of the same initial aeromagnetic data allow the maximum amount of detail to be extracted in regional structural analysis, hence additional enlarged high-resolution images are included in the accompanying Supplementary Material.

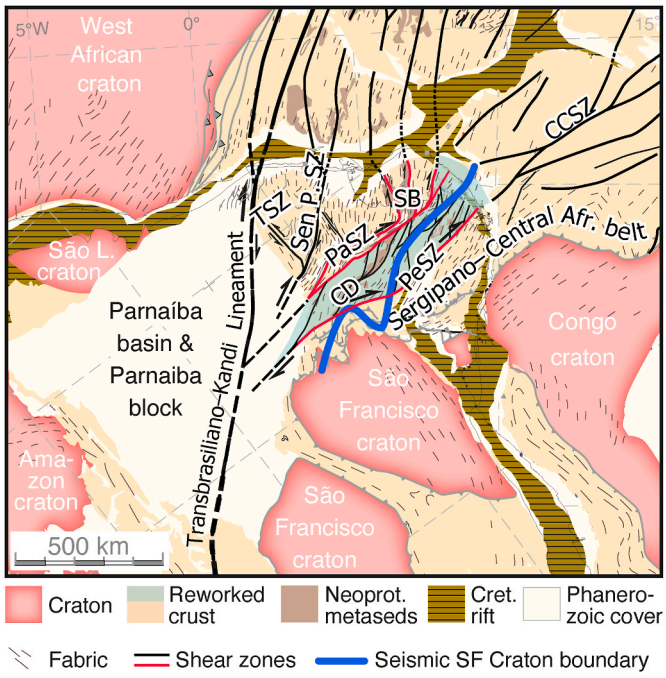

Fig. 1. Tectonic setting of the Patos and Pernambuco shear zones in Brazil, restored to the pre-drift situation at 142 Ma (from Heine, 2013) relative to the Congo craton. Key shear zones discussed in the text are marked by red lines, and the Central Domain of the Borborema province is tinted green. Blue line indicates the seismic SF Craton boundary. Cratons are shown in red. CCSZ; Central Cameroon shear zone, CD; Central domain, PaSZ; Patos shear zone, PeSZ; Pernambuco shear zone; Sen P. SB; Seridó Belt, SZ; Senador Pompeu shear zone, TSZ; Tauá shear zone. The PaSZ, PeSZ and the green-tinted Central domain define the target of this study. Current long/latitudes indicated by dashed pale gray lines so that Brazil is rotated anticlockwise with respect to Africa. (For interpretation of the references to color in this figure legend, the reader is referred to the Web version of this article.)

2. General setting of the Borborema shear system

The Borborema shear zone network in the Borborema Province developed in Archean-Proterozoic crust in the late Neoproterozoic (Ediacaran) to early Cambrian, during the regional Brasiliano–Pan-African orogenic cycle associated with the amalgamation of Gondwana (Caby, 1989; Arthaud et al., 2008; de Wit and Reeves, 2008; Van Schmus et al., 2008; Neves et al., 2021a). The Borborema Province is tectonically separated from the presently exposed São Francisco–Congo craton by the Rio do Pontal-Sergipano-Central African belt, whose main Neoproterozoic tectonic rift-related events follow either Paleoproterozoic rifting or subduction and continental arc magmatism, depending on different authors (discussed below). The Borborema Province is separated from the Amazon and West African cratons by the Ceará Central and Transbrasiliano-Kandi strike-slip system, part of the major West Gondwana orogen (Fig. 1). The latter includes a collisional event where subduction of oceanic crust during closure of the Goiás-Pharusian ocean east of Amazonia led to collision between the Amazonian and São Francisco cratons around 620-610 Ma (Fetter et al., 2003; Ganade de Araujo et al., 2014a,b). Proterozoic and older rocks of the Borborema Province are overlain by a number of Paleozoic-Mesozoic sedimentary basins, beneath which the shear zone system can be traced on aeromagnetic images.

Diverse models have been proposed for the formation of Borborema Province sequences, especially in the Central and Southern domains. The Central Domain records evidence for formation, metamorphism and deformation of a 2125 ± 7 and 2044 ± 5 Ma juvenile crust, 2.05–2.03 Ga Transamazonian metamorphism, and 1.99–1.97 Ga late-to post-

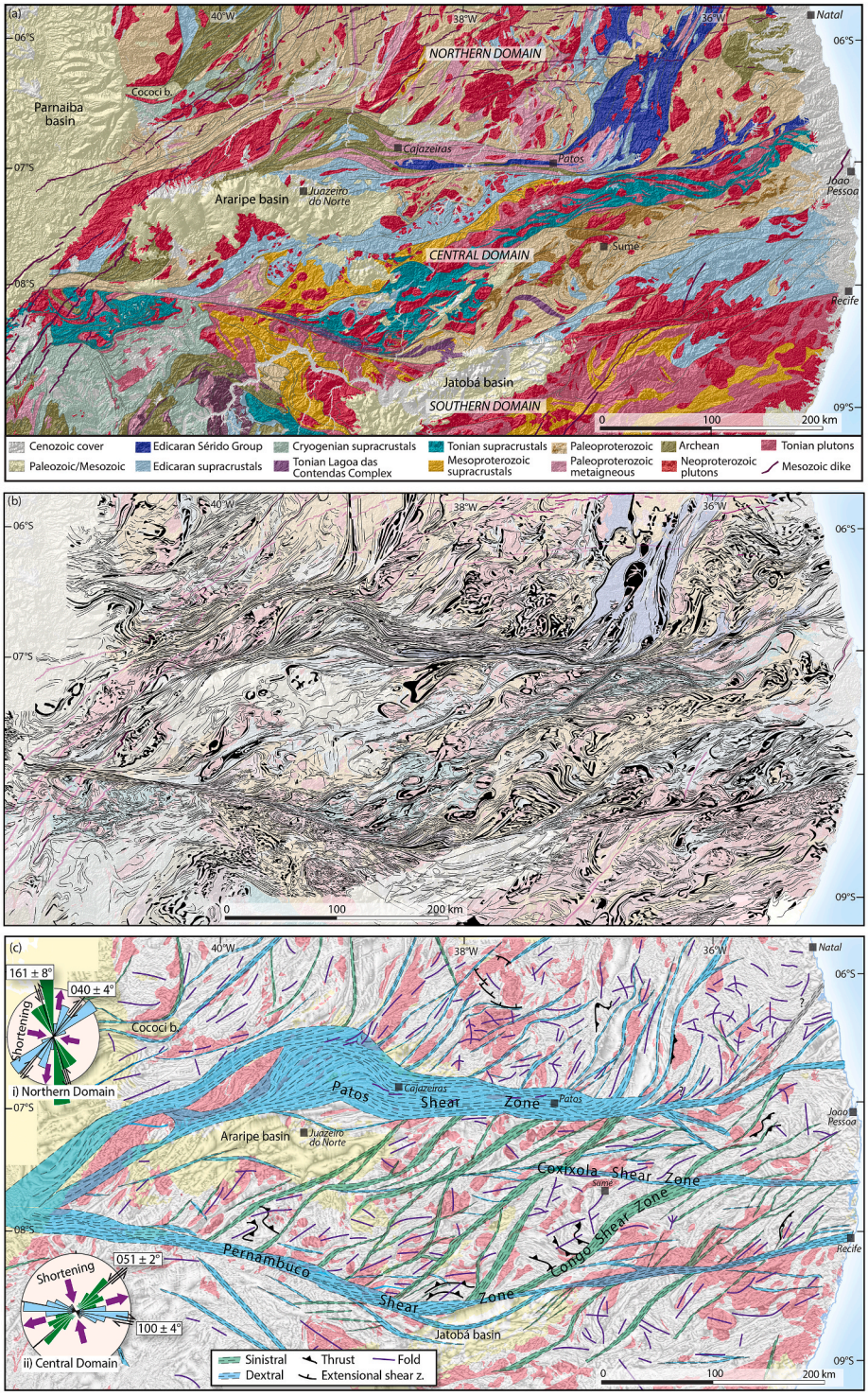

Fig. 2. (a) Geologic map of the main Borborema region, based on public maps by the Brazilian Geological Survey. Mesozoic dikes are interpreted from magnetic anomaly maps in Fig. 3. (b) Manual interpretation of the Ternary anomaly image, on top of the geologic map in (a) (dimmed). (c) Interpretation of shear zones and their kinematics, mainly from aeromagnetic images. Rose diagrams show orientation of dextral and sinistral shear zones in the Northern and Central domains, respectively. Axial trace of folds as interpreted from aeromagnetic images are also shown. Note the differences in shortening direction for the two populations.

Transamazonian magmatism (Neves et al., 2006). Mafic-ultramafic rocks of the Carmo Suite and felsic rocks of the Pedra d'Água Suite of the Central Domain (Santos et al., 2015) overlap formation of the N-S trending 2.2 to 2.0 Ga Salitre Rift in the N São Francisco Craton (de Paula Garcia et al., 2021). Magmatic events and amphibolite facies metamorphism in orthogneisses and supracrustal rocks (Neves et al., 2006) in the Central Domain suggest an E-W rift, contemporaneous with the Salitre Rift, initiated in the Paleoproterozoic, where the change of rift orientation and mafic-ultramafic magmatism suggest the possibility for a mantle plume, although more research is required to confirm this.

The Southern and Central domains subsequently went through a history of intracontinental Tonian rifting from ~1000 to 820 Ma, reactivating the Paleoproterozoic rift, which may have culminated in, or have been further reactivated between 630 and 610 Ma. This was a time of deposition of supracrustal sequences, formation of flat-lying foliations and Brasiliano high-T/low-P metamorphism (Caby et al., 1995; Caby and Atthaud, 1986; Neves et al., 2000, 2005, 2016), again consistent with an extensional tectonic setting. Other models invoke one or more subduction-accretion events (e.g., Oliveira et al., 2010; Santosde Oliveira et al., 2021), but as Neves et al. (2016) contend, no conclusive

evidence is seen for a subduction-related magmatic arc on the N margin of the São Francisco Craton between 1000 and 920 Ma in the SW part of the Southern Domain (Caxito et al., 2020) or for the oceanic subduction and collision between 635 and 580 Ma suggested by Brito Neves et al. (2016) and Caxito et al. (2014, 2017, 2021). Indeed, seismic tomographic and gravity data suggest that the São Francisco Craton continues beneath the southern, especially southeastern part of the Borborema Province (Rocha et al., 2019; Ganade et al., 2021).

Internally, the Borborema Province underwent intracontinental deformation during this entire Neoproterozoic period, and the general understanding is that multiple intraplate rifting events described above were followed by subduction-related orogeny along the northern margin of Borborema (the Ceará Central domain north of the Patos Shear Zone) around 620–600 Ma, followed by transcurrent shearing and magmatism mainly between 590 and 570 Ma (Archanjo et al., 2008, 2011; Neves et al., 2015, 2016; Ganade et al., 2021). This time interval is largely based on dating of several of the many granitic bodies in the province (Ganade de Araujo et al., 2014b; Ganade et al., 2021; Ávila et al., 2019). Along with the intrusion of mostly granitoid bodies, the Borborema crust underwent partial melting at the time of shearing, particularly in the Northern Domain, within the Patos shear zone and in the central and western part of the Pernambuco shear zone. Basement rocks in the Central domain are also migmatized, but the age of this migmatization is not well constrained. The widespread partial melting underscores the hot nature of the tectonic events in the Ediacaran and the weak nature of the crust (Cavalcante et al., 2016).

Past research has established a bulk dextral sense of displacement on the Patos and Pernambuco shear zones (e.g., Vauchez et al., 1995; Corsini et al., 1991; Viegas et al., 2014; Archanjo et al., 2021). Most authors also show a dominance of dextral shear on NE-striking shear zones north of the Patos shear zone, whereas there are highly conflicting interpretations of the sense of displacement on similarly oriented shear zones in the Central Domain. For example, a sinistral sense was assigned by Archanjo et al. (1999), Neves et al. (2005, 2012, 2021b), Ganade de Araujo et al. (2014b) and Pereira et al. (2019), while Tommasi et al. (1995) and Vauchez et al. (1995, 1998), Vauchez and Egydio-Silva (1992), Caxito et al. (2016, 2020, 2021), Oliveira and Medeiros (2018) and Liu et al. (2019) infer dextral shearing for the same

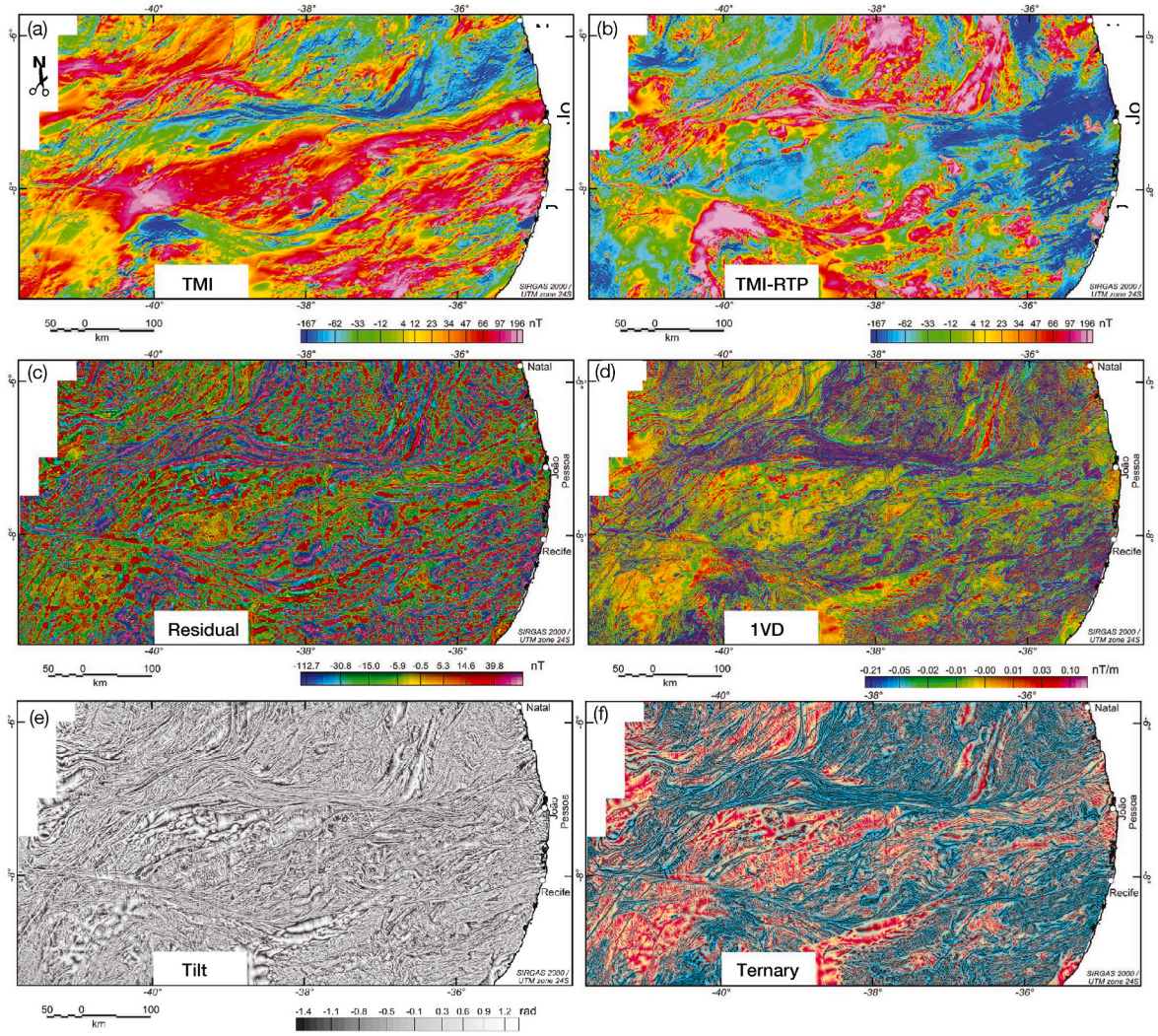

Fig. 3. Processing and enhancements of aeromagnetic data: (a) Original aeromagnetic data (TMI). (b) Reduced to the pole (TMI-RTP) with the same color scale as (a), which matches mapped geology in Fig. 2a. (c) Short wavelength components edge-enhanced using its theta angle. (d) The shaded first vertical derivative (1VD). (e) Tilt angle. (f) Ternary image combining gradients and their ratios, assigned to 3 colors. Image (c) has far less noise than (d) and is best for relating to surface lithology, whilst images (e) and (f) best highlight structures. The effect of sediments of the Tucano-Jatobá basin is more apparent in the 1VD image (d) than in the short wavelength (residual) image in (c). Note that the white rectangle with titles is an area of no aeromagnetic data at this resolution. Enlarged high resolution images, additional treatments, and enlarged comparisons between TMI and TMI-RTP images and mapped geology and in profile are provided in Supplementary Material. (For interpretation of the references to color in this figure legend, the reader is referred to the Web version of this article.)

structures. Our study attempts to clarify these disparate interpretations, and we demonstrate that these prominent NE-striking shear zones in the Central Domain are clearly sinistral.

3. Borborema aeromagnetic data, processing and applications

3.1. Aeromagnetic data and its enhancement

The aeromagnetic data employed in this project was a compilation produced by the Brazilian company GSM Geophysics of data acquired in 2008 through a joint effort by the Brazilian Geological Survey and the Ministry of Mines and Energy along variably but mainly NW-SE oriented flight lines at a 100 m nominal height and with a 500 m spacing, interpolated on a 126 m grid. The initial Total Magnetic Intensity (TMI) data in Fig. 3a and Supplementary Material Fig. 1a (Supplementary Material figures are subsequently referred to as SM1a, etc.) show high (red) to low (blue) anomalies that relate to rock magnetic susceptibility, largely due to the presence of magnetite and other magnetic minerals (see Isles and Rankin, 2011 and Dentith and Mudge, 2014 for explanations of the magnetic geophysical technique). In order to use this data for lithologic and structural mapping, a reduction to the pole (RTP) algorithm was applied to locate the magnetic anomalies above their causative rock bodies (Fig. 3b, SM1b). Without this initial RTP treatment, large magnetic highs have commensurate large magnetic lows, giving a false impression of different juxtaposed high and low magnetic values for those not used to interpreting geophysical data. Additionally, anomalies are laterally displaced from their sources and false more E-W trends sometimes appear in the data that are not validated by mapping, at the expense of more N-S structures. Some folds and planar structures that are not recognizable from the original TMI map are then identified; these are largely consistent with the geologic map (Fig. 2a), but not completely, because geologic maps show surface expressions in areas of outcrop while magnetic images also contain information from the subsurface (see Isles and Rankin, 2011). Total field magnetic images therefore reflect lithologic and structural patterns that are representative for a volume of crust in comparison to classical geologic maps based on surface observations. Volumes corresponding to different source depth ranges can, however, be extracted using filtering techniques in the frequency domain based on changes of slope of the radially averaged power spectrum (Spector and Grant, 1970; Likkason, 2011), hence near surface short wavelength ("residual") components that, with source depth less than ca. 10 km, relate more directly to surface geologic maps were separated from deeper crustal, long wavelength components (Fig. 3c). This method is preferred to more commonly used vertical derivatives (e.g. 1VD; Fig. 3d) as residual potential field images contain less noise and one has a control on source depths portrayed; the images also reflect measurements in a given depth range in nT instead of gradients (i.e. nT/m) as in the 1VD. RTP aeromagnetic data was also converted to pseudo-gravity potential (Baranov, 1957; more commonly shorted to pseudo-gravity), a treatment based on Poisson's relationship between gravitational and magnetic potential fields (Poisson, 1826) assuming constant magnetization. Pseudo-gravity (Fig. 4) accentuates deep crustal domains due to vertical integration incorporated in its calculation. Especially where their edges are enhanced (Fig. 4b and c), pseudo-gravity depth slices provide complementary information to that provided by standard treatments of aeromagnetic and gravity data (Cooper and Cowan, 2005; Jekeli et al., 2010).

Both residual magnetic and pseudo-gravity images were enhanced for structural interpretation. The tilt angle (= arctan of the ratio of the vertical derivative and the total horizontal derivative; Miller and Singh, 1994; Salem et al., 2007, as in Fig. 3e) and theta map/angle (Wijns et al., 2005) derived from the analytic signal, itself calculated from horizontal and vertical gradients (Roest et al., 1992), highlight contacts and structures such as faults and ductile shear zones, and enhance subtle features in aeromagnetic data. Using the theta angle to highlight edges (contacts) in aeromagnetic data, as in Fig. 3c, and pseudo-gravity data

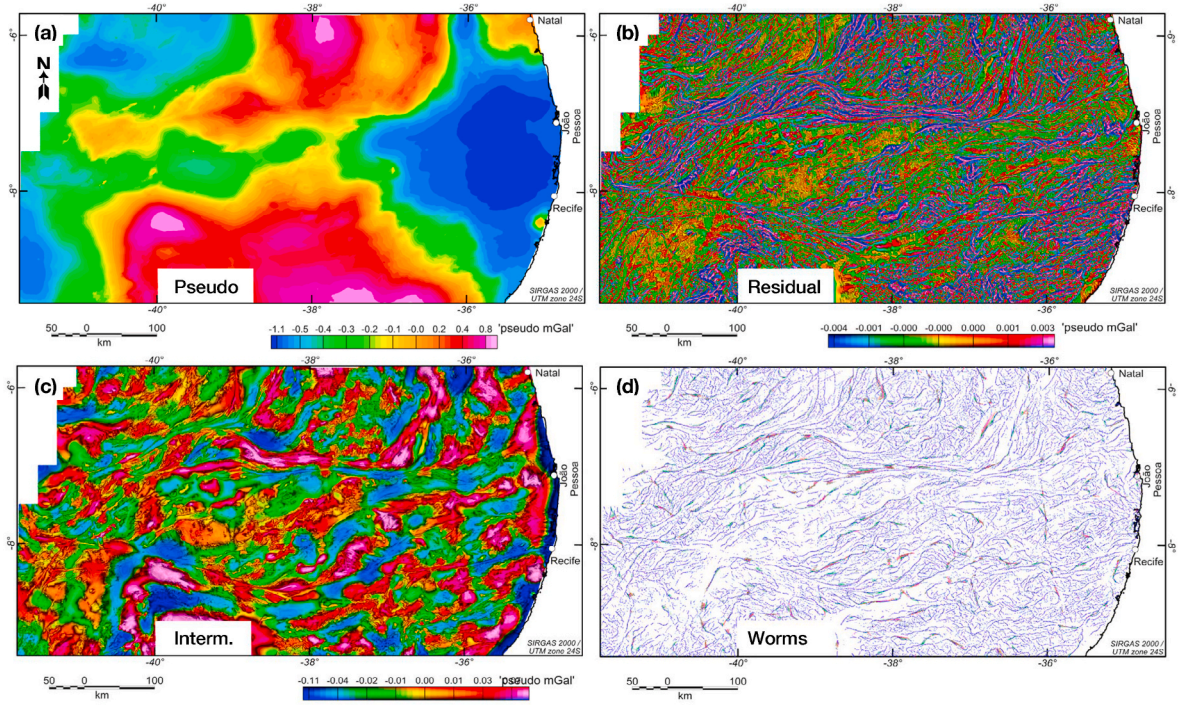

Fig. 4. Pseudo-gravity and its enhancements. (a) Pseudo-gravity calculated from aeromagnetic data enhances deep features. (b) Short wavelength (residual) components highlight features closer to the surface; although very similar to the residual aeromagnetic image, removing some surface to near-surface effects better highlights some features. See enlarged comparisons in Supplementary Material. (c) Intermediate wavelength components = intermediate depth slice. See Supplementary Material for corresponding power spectra and depth ranges of (a) to (c). (d) Pseudo-gravity worms, the edges in horizontal gradient calculated at different depths (i.e. different levels of upwards continuation) highlight geological contacts across which there was a marked difference in magnetic susceptibility.

(Fig. 4b and c) is especially advantageous close to the equator to help overcome any distortion arising from the reduction to the pole (Wijns et al., 2005). More examples of the use of theta angle images for portraying complex fold geometries are included in the Supplementary Material. Ternary combinations of different gradient-based images (Fig. 3f) increase contrast, and these are especially useful in portraying foliation trajectories (Fig. 5) and to differentiate between different types of intrusions.

Multiscale edges in the horizontal gradient of pseudo-gravity data for different source depths, commonly termed "worms" (a wavelet analysis technique developed by Hornby et al., 1999, conceived independently, although purely theoretically, by Moreau et al., 1997). Pseudo-gravity worms highlight sharp magnetic contrasts that result from discontinuities or interfaces between different lithologies or geologic structures such as faults, unconformities, or intrusive contacts (Holden et al., 2000). Worms also portray differences between near-surface and deeper structures (Fig. 4d), and also provide a rapid means to estimate dips of faults or lithologic contacts. Further details on 'worming' methodology are provided by Hornby (2019) and Holden et al. (2000), and a regional example of pseudo-gravity ('magnetic') worms is given by Vos et al. (2006). Worms also provide a means of verifying reduction to the pole calculations which may be problematic if remanent magnetization is present or, as for NE Brazil, areas close to the equator. Comparison between pseudo-gravity worms calculated from RTP aeromagnetic data with geologic contacts mapped in the field confirms the validity of undertaking RTP for our study area (see SM6-7).

3.2. *Aeromagnetic expression of Brasiliano shear zones in the Borborema Province*

In addition to complementing previous regional mapping, enhanced aeromagnetic images provide hitherto unknown details of shear zone kinematics and geometries, fold styles and orientation, strain distribution, and controls on shear localization. The ternary gradient images shown in Figs. 3f and 6 enhance the foliation trajectories to produce a high-contrast structural image that portrays the structural shear zone pattern particularly well. This image tends to display felsic rocks in red-orange, and supracrustal rocks in tones of blue and black. Neoproterozoic and younger metasedimentary rocks with rather uniform magnetic properties have a bright and uniform expression. Paleozoic-Mesozoic basins attenuate the magnetic signal from underlying units, but they can still be recognized to some degree, for instance under the Araripe and Parnaíba basins. A modified version of this map (included in Supplementary Material) that provides another visual representation of structure was used together with Fig. 3f for structural interpretation. A manual structural interpretation based on the enhanced residual aeromagnetic anomaly maps and an interpretation of main shear zones and their kinematics is shown in Fig. 2b and c, respectively. Mesozoic dikes have been excluded in these map interpretations.

Comparing the processed aeromagnetic images and the manual structural interpretation with the surface geologic maps produced by the Brazilian Geological Survey, we see a clear correlation between lithologic boundaries and RTP aeromagnetic anomalies (compare Fig. 2a with 2b and images in Fig. 3). Several of the granitoid bodies are easily correlated, as are fold and shear zone patterns. The aeromagnetic images also reveal how the Patos and Pernambuco shear zones continue westwards underneath the Parnaíba basin. Fig. 6 provides an example of an enlarged area to show the expression of shear zones on different enhancements. The increased contrast in the ternary image better portrays foliation trajectories. Overlaying a simplified interpretation of ductile shears from the ternary image on the intermediate wavelength pseudo-gravity image in Fig. 6c (highlighting deeper lithologic domains) in Fig. 6d shows that several NE-SW to ENE-WSW sinistral, antithetic shears are controlled by lithologic domain margins. The ternary image in Fig. 6b also clearly shows the location and differences in deformation of felsic rocks not so apparent in the initial, residual image in (a): the orange-colored granitoid body at the left (W) margin is unfoliated but cut by fractures whereas many other layers in orange are highly foliated. Further detailed comparisons are given in the Supplementary Material.

4. The Patos and Pernambuco shear zones

The roughly E-W trending Patos and Pernambuco shear zones are the main features of the shear network of the Borborema Province (Figs. 1 and 2). They are up to a few tens of kilometers wide and characterized by steep foliation and dextral offsets, although the Patos shear zone is thicker and internally more complex. Calculations of average dips from the surface to 5 km depth based on pseudo-gravity worms show E-W shear structures within the Patos shear zone dipping between ca. 50° S and 78° S, although in its western part one shear zone between two S-dipping shear structures dips northwards between ca. 45° and 65°. Shear structures in the western half of the Pernambuco shear zone dip between ca. 40° NNE and 55° NNE, while no clear dips could be established in its eastern half. The Patos and Pernabuco shear zones can be traced continuously for more than 700 km in length; aeromagnetic data suggest they continue southwestward beneath the Parnaíba Basin and merges with the Transbrasiliano lineament (de Castro et al., 2016). In tectonic reconstructions, the Patos-Pernambuco shear system correlates with shear zones of the same age on the N margin of the Congo Craton, hence their total original length was at least 2000 km (Fig. 1; Caby, 1989; de Wit at al., 2008; Julios et al., 2020). Occurrences of unsheared Cambrian to Cretaceous sediments (Fig. 2) provide a minimum age for the ductile shearing history. They are, however, affected by brittle deformation associated with the Cretaceous rifting that led to the pre-opening rifting

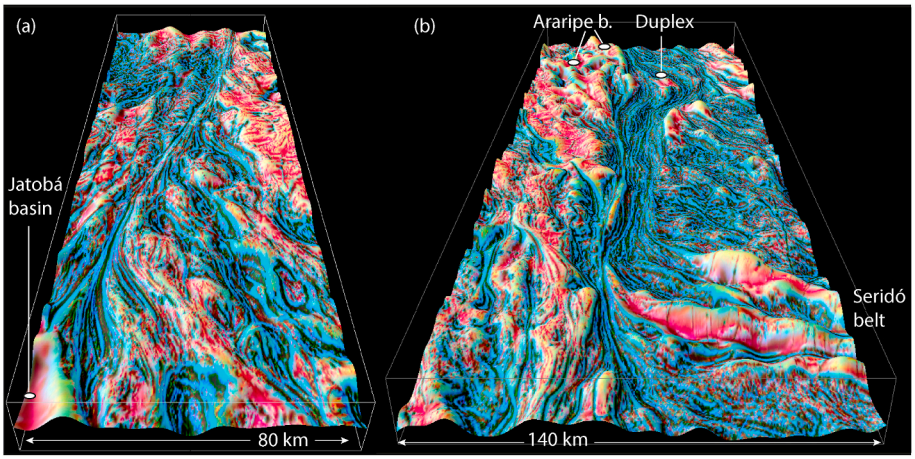

Fig. 5. 3D perspective view of the ternary magnetic anomaly pattern (Fig. 3f) over the Pernambuco (a) and Patos (b) shear zones, looking west. The pattern reveals the structure of the shear zones very well, confirming the overall dextral rotation of fabrics into the two main shear zones. Warm and cool colors have been given a positive and negative relief, respectably, using the imageJ software (https://imagej.nih.gov/ij/). (For interpretation of the references to color in this figure legend, the reader is referred to the Web version of this article.)

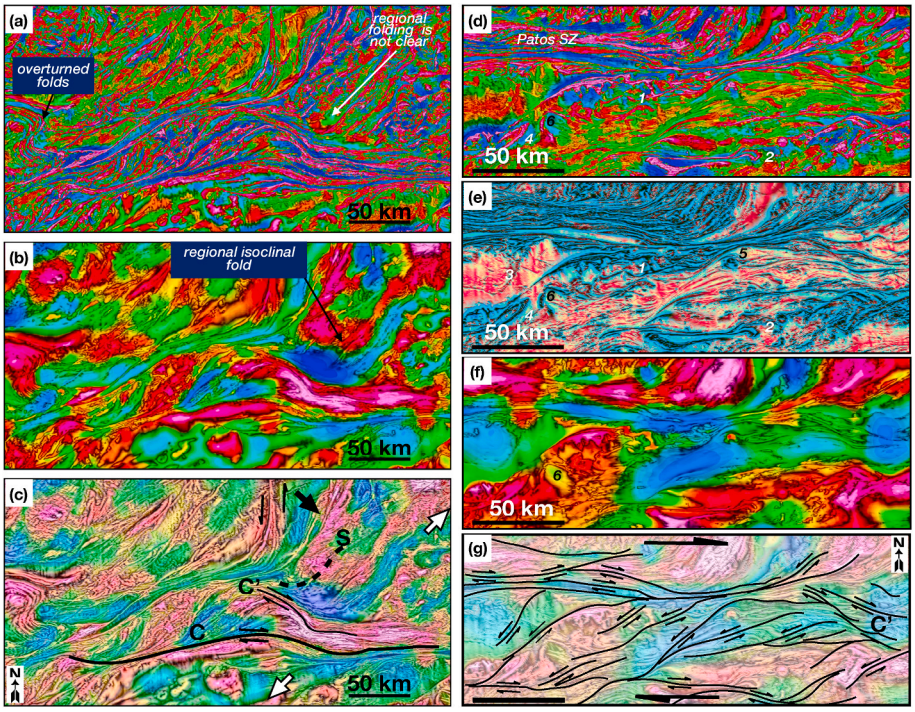

Fig. 6. Examples of enlarged areas to show how a combination of enhancements of magnetic and pseudo-gravity derived from the same original data aids structural interpretations. (a)–(d) show how both aeromagnetic and pseudogravity data provide complementary information on regional folding in the Northern Domain N of the Patos shear zone and (e) to (g) provide an example of the expression of shear zones and controls on their localization in the Central Domain (see Supplementary Materials for location maps). Although there are hints of a possible fold closure, the edge enhanced residual aeromagnetic image in (a) gives little indication for the presence of regional isoclinal folding in this part of the Northern Domain, and no regional folds are shown on CPRM geological maps in this enlarged area. A regional-scale isoclinal fold is, however, clearly portrayed by the intermediate pseudo-gravity image in the top right (NE corner) of (b), hence NNE-striking foliations in (a) represent a transposed tectono-metamorphic fabric axial planar to regional folds. Hints of this foliation are seen in (b), but the fold-axial planar foliation relationships are best seen in combining the residual tilt angle image in gray with the pseudo-gravity image in (b) in (c). The axial trace away from the shear zone suggests an S/C relationship consistent dextral shear. The NW-SE shear zone is oriented with respect to C equivalent to a C′ shear in a mylonite." The short wavelength aeromagnetic image in (d) and a ternary image combining different gradients and their ratios in (e) highlight near surface foliations and their deformation, e.g.: (1) folds formed during back rotation between antithetic shears, (2) offset isoclinal fold whose axial surface has been reoriented into parallelism with a dextral shear zone, (3) fracturing within a more competent intrusion, (4) fold with axial traces at 45° to shear zone margins, (5) foliation asymmetry around an intrusion akin to a sigma porphyroclast. The intermediate wavelength ternary image in (f), and a paler copy in (g), highlights different lithologic packages. This image better shows the complete outline of an intrusion at 6, which could have easily been misinterpreted (without geological maps) as a fold closure. The shear zone interpretation in (g) shows that whilst dextral synthetic (C′) shears occur within lithologic units, lithologic contacts control the orientation of several antithetic sinistral shears. Color ramps as in Figs. 3 and 4. (For interpretation of the references to color in this figure legend, the reader is referred to the Web version of this article.)

of the Atlantic margins.

4.1. The Pernambuco shear zone

The Pernambuco shear zone is composed of two almost straight segments (west and east Pernambuco shear zone, separated by the Mesozoic Jatobá Basin) with a rather abrupt but continuous change in orientation at the northern boundary of the Jatobá basin (Figs. 2 and 3). The shear zone stands out as a marked and continuous lineament on the aeromagnetic images that separates rocks of different ages and of different lithologies and magnetic properties (Fig. 3). It has previously been suggested that these two segments are unconnected and associated with relatively limited displacements (Vauchez and Egydio-Silva, 1992; Neves and Mariano, 1999). However, the magnetic data (Fig. 3) and structural considerations presented here support the view that the segments are connected and form a single large-displacement ductile shear zone, and that one or two sub-parallel shear segments occur south of the east Pernambuco shear zone (Fig. 7).

The Pernambuco shear zone is a predominantly ductile (plastic) structure with classic rotation of foliations and lithologic units into the zone, particularly well-developed along its northern margin (Fig. 7). The shear zone contains evidence for both high- and low-temperature deformation (Neves and Mariano, 1999; Castellan et al., 2020), suggesting that the shear zone was active at a range of thermal conditions. For the eastern Pernambuco shear zone, Castellan et al. (2020) estimate conditions of 0.475 ± 0.03 GPa and 526 ± 9 °C in synkinematic granitoids of the Caruaru domain and 0.59 ± 0.1 GPa and 437 ± 17 °C in the Gravatá domain further east. Brittle reactivation of the ductile gneissic or mylonitic fabric is also seen, and a U-Pb age of calcite fibers on one such normal-sense slip surface provided a lower Cretaceous age of 135 ± 5 Ma, taken to date the time of reactivation (Miranda et al., 2020). This is the time of Mesozoic rifting of the region, with formation of the nearby Jatobá basin of the Rêconcavo-Tucano-Jatobá rift system.

The shear zone thickness is here defined as the distance between points where the external fabric starts to rotate into the shear zone. This thickness is ~20 km in the west, where the Pernambuco shear zone gets covered by Silurian and younger rocks of the Parnaíba basin. It then decreases to 10 km near the W margin of the Jatobá basin, where part of the shear zone has been faulted and covered by the clastic basin fill. Eastwards from the Jatobá basin, the zone seems to be only around 5 km thick on average, getting close to 10 km again near the Atlantic coast. This could reflect an eastward drop in displacement from the location of the Jatobá basin. Such an eastward drop in displacement was explained by a northeastward splaying of the shear zone (Vauchez and Egydio-Silva, 1992). However, this model predicts the splays to be dextral, whereas they are clearly portrayed as sinistral on the aeromagnetic images. Instead, our study shows that dextral displacement is accommodated on several dextral shear zones parallel to and S of the east Pernambuco shear zone with both N and S dips (Figs. 2b and 3).

The magnetic images also show a southern shear zone segment that underlies the basin, forming a lens-shaped geometry with the main Pernambuco trend. We interpret this lens-shaped geometry as a possible linkage structure, where the two main segments of the Pernambuco shear zone initiated as individual shear zones of slightly different orientations and linked during mutual propagation (Fig. 7e–f) – a lengthening mechanism that is extremely common for faults (e.g., Walsh et al., 2003; Fossen, 2016), but also demonstrated for ductile shear zones (Fossen and Cavalcante, 2017).

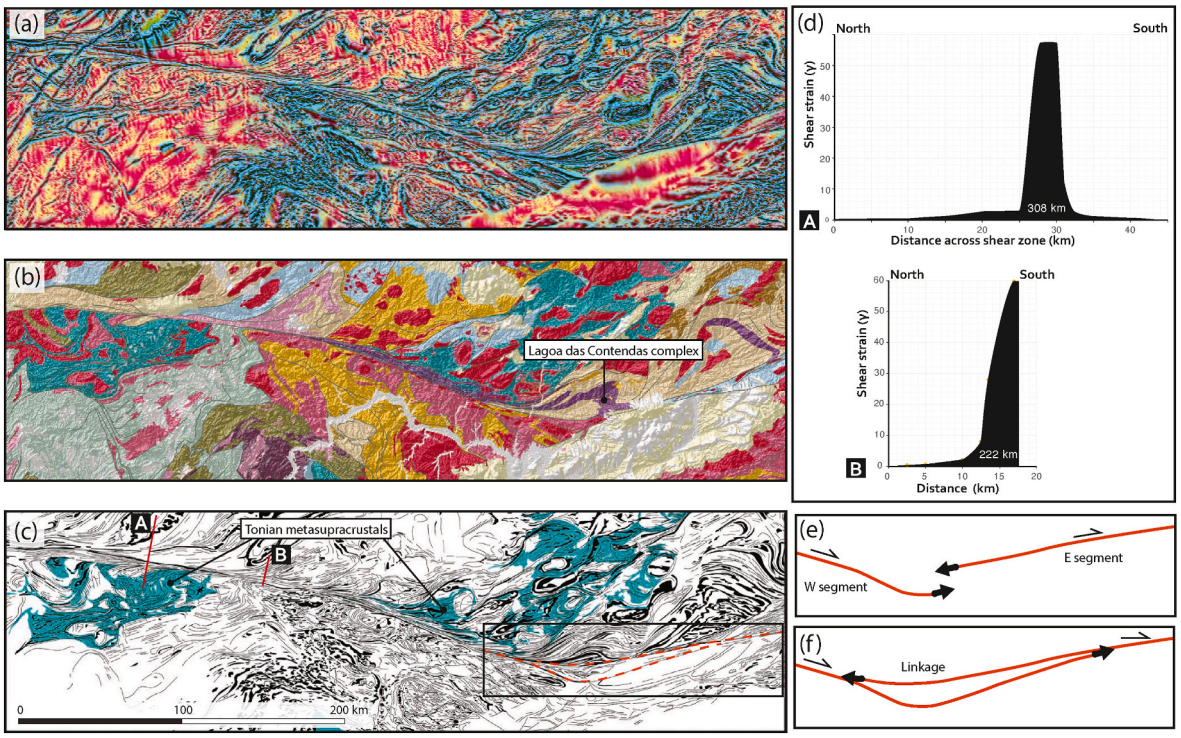

Fig. 7. Pernambuco shear zone. a) Enhanced magnetic anomaly map showing the structure of the east and central part of the shear zone. (b) Lithologic map (see Fig. 2a for legend). (c) Structural interpretation. (d) Shear strain profiles and displacement assuming simple shear. (e–f) Simple linkage model for the connection between the east and west segments of the Pernambuco shear zone. Full black arrows indicate propagation directions.

A dextral sense of shear is consistently observed along the Pernambuco shear zone. This is clearly expressed by rotation of foliations and lithologic units into the shear zone that can be seen both from the geologic and aeromagnetic anomaly maps (Fig. 7). This shear sense is also evident from outcrop to microscale structures as observed in the field and thin section (e.g., Neves et al., 2000).

4.1.1. Horizontal displacements

The aeromagnetic data helps to constrain the thickness of the shear zone and to visualize the pattern of rotation of host-rock fabrics into the zone. This pattern can be utilized to construct strain profiles across the shear zone, as has been done along two sections across the western segment where the pattern is particularly clear (Fig. 7). We assumed simple shear deformation and employed the equation for rotation of preexisting passive markers (Ramsay 1980):

$$\cot\beta' = \cot\beta + \gamma$$

where β is the angle that the marker initially makes with the shear zone, and β' is the new angle whose value will depend on the local shear strain (γ). It is possible that the shear zone deformation deviates from simple shear, which would introduce an error to the strain estimates. However, the large offset of this shear zone suggests that the simple shear component is completely dominating, and the largest error comes from accurately determining the angle β' where strain is high. In this portion of the zone the foliation is almost parallel to the shear zone, and small variations in the angle make large differences in calculated shear strain. We have used the assumption that the strain in the central part of the zone is as high as it is where we lose control as we move through its margin, i.e. $\gamma \approx 50$–60. In other words, we made the strain profile flat across the inner and highest strained part of the zone. The results (Fig. 7d) show classical shear strain profiles, and integration of shear strain over the width of the zone (Ramsay 1980) yields estimates of around 308 and 222 km.

This amount of displacement (222–308 km) is corroborated by the offset of units along the shear zone. In particular, the Tonian Lagoa das Contendas complex, shown in Fig. 7b in violet color, appears to have been displaced around 200 km along the zone before vanishing in a highly sheared state within the zone. If we consider other Tonian subracrustal units on both sides of the shear zone, an offset on the order of 200 km is also indicated (Figs. 7c and 8c). Paleoproterozoic gneissic units also show an apparent lateral offset in excess of 200 km (Fig. 8b). A similar estimate was made by Ganade et al. (2021) based on the regional distribution of radiometric model ages. In summary, the consistency between our structural analysis and offset patterns of rock units leads us to the conclusion that the ductile Ediacaran strike-slip displacement of the Pernambuco shear zone is about 200–250 km.

4.2. The Patos shear zone

The more than 700 km long Patos shear zone is located almost 200 km north of the Pernambuco shear zone, in the middle of the Borborema Province (Fig. 1). A NE-trending segment links the Western Patos shear zone with the Pernambuco shear zone and continues under the eastern part of the Parnaíba basin to merge with the Transbrasiliano lineament (de Castro et al., 2016). In our main study area, the Patos shear zone continues eastwards from the Parnaíba basin for ~700 km (Fig. 2); Fig. 9a–c shows an enlarged image, geologic map and interpreted internal geometry of its central section. An up to 70 km wide strike-slip duplex (Fig. 10) marks the change from its NE-trending western section to the E-W central section (Corsini et al., 1996), possibly with another, somewhat smaller duplex to the southwest (ca. 40.5°W, 7.5°S; Fig. 3e and f). The latter is partly covered by Phanerozoic deposits but discernible from the aeromagnetic data.

Eastwards the shear zone continues as the straight central segment of around 30 km thickness until it bifurcates into several E-W to NE-SW trending branches. The aeromagnetic images show that one branch continues more or less straight towards the coast. Another set of branches is located along the NNE-trending Seridó belt (Fig. 9). The

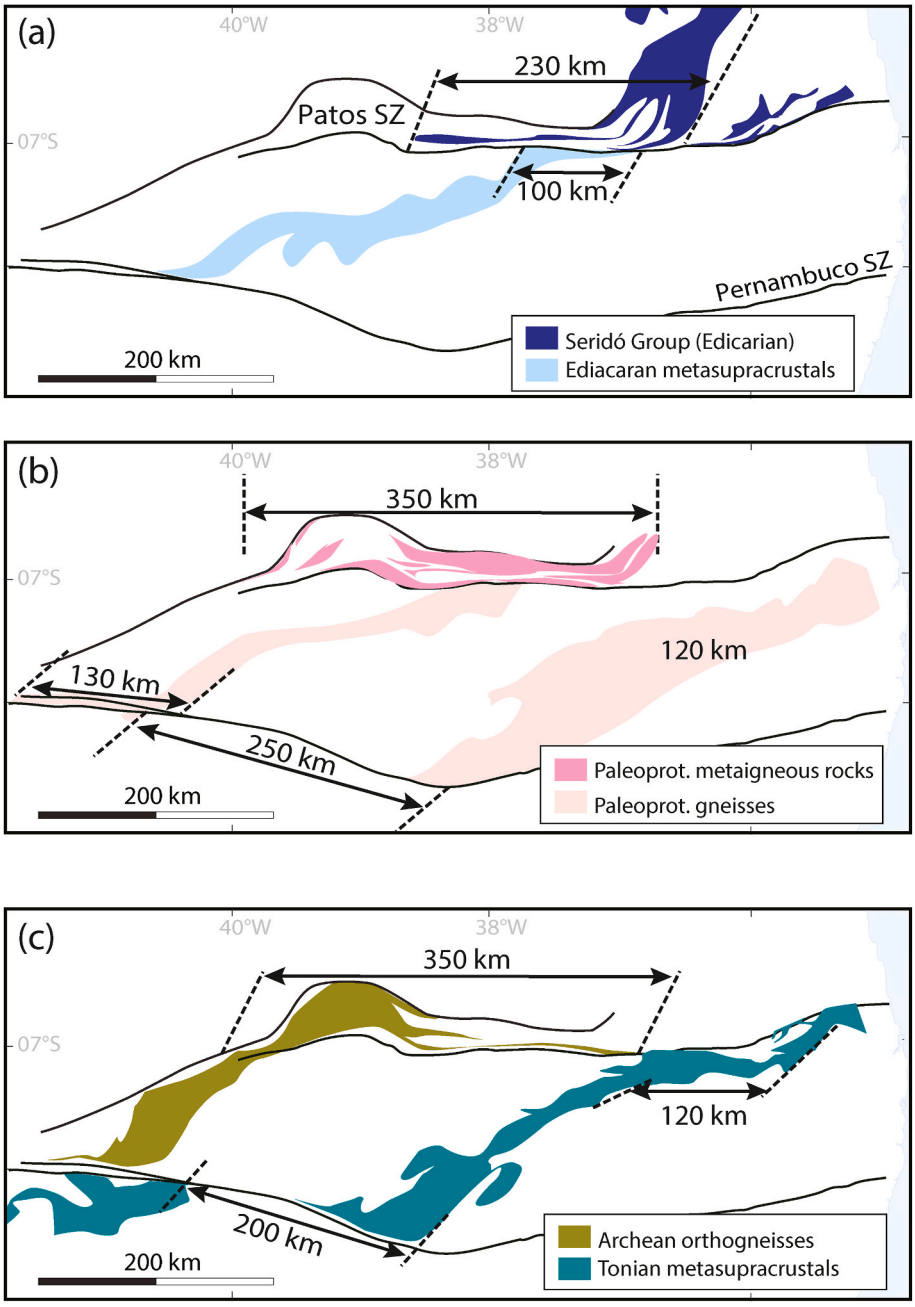

Fig. 8. Distribution of rock units across the Pernambuco and Patos shear zones and their indication of apparent lateral displacement. (a) Deflection of the Seridó Formation from the north into the Patos shear zone indicates a minimum of 230 km apparent offset. Ediacaran supracrustals are sheared 100 km along the south margin of the Patos, suggesting that the total offset of the Patos is much more than 100 km. (b) Paleoproterozoic metaigneous rocks are sheared for 350 km along the Patos shear zone, indicating a minimum of 350 km offset. Paleoproterozoic gneisses in the east Pernambuco first reappear in the south wall some 250 km to the west. The western zone of Paleoproterozoic gneisses is sheared 130 km along the Pernambuco shear zone. (c) Archean units and their apparent minimum offset of 350 km along the Patos shear zone. Tonian supracrustals indicate 200 km offset along the Pernambuco shear zone. Each estimate is uncertain, but together they are internally consistent and also consistent with strain-based displacement estimates (Figs. 7 and 9).

Seridó belt is interpreted as a high-T transpressional segment with peak metamorphism around 575 Ma in which deformation is partitioned into a set of subparallel NNE-trending dextral shear zones, thrusts and folds (Archanjo and Bouchez, 1991; Archanjo et al., 2002, 2013; Domingos et al., 2020; Cioffi et al., 2021).

A characteristic feature of the sheared rocks within the Patos shear zone is the range in thermal conditions recorded during deformation. In its main E-W segment from Cajazeiras past Patos (Fig. 2c), the main portion of the shear zone is hot with the occurrence of syn-kinematic metatexites and diatexites that formed together with high-temperature banded gneisses, where the melt has been dated to around 565 Ma (Viegas et al., 2014; Archanjo et al., 2021). Temperatures of 550–600 °C at 0.3–0.4 GPa were determined from metamorphic assemblages in the Seridó Belt ca. 60 km N of the Patos shear zone (Cioffi et al., 2021). However, its southern part is constituted by low-temperature mylonites. It is not clear if these variations in thermal conditions are due to differential syntectonic exhumation or migration or localization of deformation during regional cooling. It has been suggested that the shear zone acted as a vertical conduit for melt that would weaken and heat it (Cavalcante et al., 2016), which could also cause lateral thermal variations. Transpressional deformation is suggested for internal parts of the strike-slip duplex, where thrusting appears to be synchronous with the overall strike-slip motion (Corsini et al., 1996). Overall, however, we consider the Patos shear zone to be approximately simple shear. The consistent dextral sense of shear (little evidence of conjugate shear bands) exhibited by abundant field-scale kinematic indicators (Fig. 7) supports this view.

4.2.1. *Relationship between regional folding and shearing N of the Patos shear zone*

The area N of the Patos shear zone, enlarged in Fig. 6a–c, shows that whilst in the NE corner of the residual aeromagnetic image in (a) a

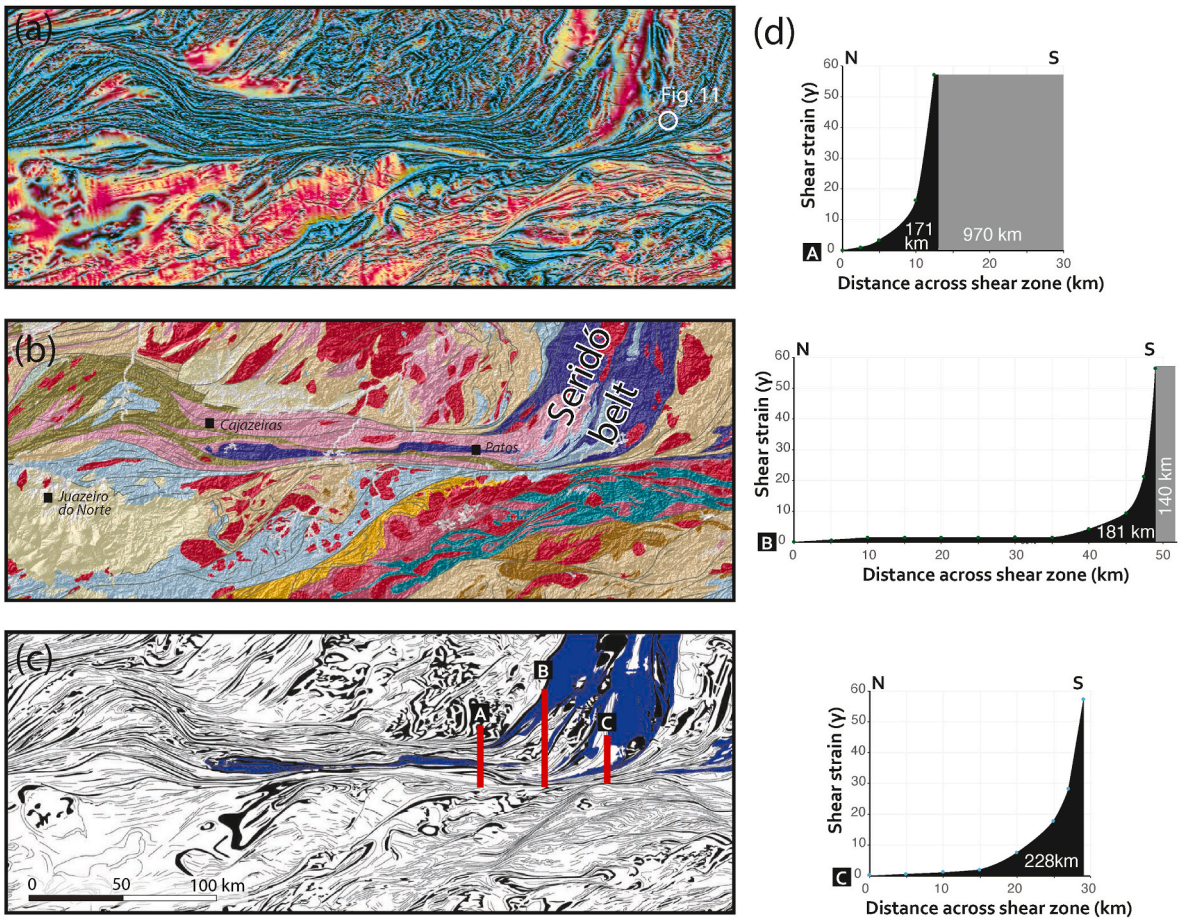

Fig. 9. Patos shear zone. (a) Enhanced magnetic anomaly map revealing the structure of the shear zone. (b) Lithology (see Fig. 2a for legend). (c) Structural interpretation, with sections analyzed for strain and displacement in (d). Gray areas in (d) are high-strain parts of the profile where the foliation is at a very low angle to the shear zone, and therefore uncertain.

foliation trending NE-SW appears to be sheared into parallelism with the Patos shear zone, the intermediate wavelength pseudo-gravity image (Fig. 6b) clearly portrays a very tight to isoclinal overturned synform with NE-dipping axial surface, thickening in the hinge and/or thinning in the limbs ("regional isoclinal fold" in Fig. 6b). The fold axial trace and shear zone thus define a regional S-C relationship (as described by Ramsay, 1967). This fold was not shown on the geologic map of the Borborema Province in Fig. 2 nor in other enhancements of aeromagnetic data in Fig. 3c–e. Folds with similarly oriented axial traces are also observed in regional pseudo-gravity data in the Northern Domain outside our study area. This is an excellent example of how significant regional folds may easily go unidentified in high grade terrains, as foliations mapped in the field and conventional enhancements to show near surface features (such as the most commonly used first vertical derivative, 1VD) are tectonic fabrics where lithologic layering is transposed into parallelism with fold axial surfaces. A similar example in another high-grade gneiss terrain is portrayed in pseudo-gravity data by Harris (this volume).

4.2.2. *Internal structures and kinematics of the Patos shear zone*

The rotation of external fabrics into the shear zone and synthetic dextral C′ shears indicate dextral kinematics within the main shear zone, although merging shear zones of the Central Domain give sinistral shear along parts of its southern margin. Dextral kinematics are also consistently observed in the field (Fig. 11) and thin section, associated with subhorizontal lineations and a steep shear zone foliation in outcrop (although pseudo-gravity worms indicate that dips may shallow with depth). As observed from the processed aeromagnetic maps, asymmetric folds occur in several places. A particularly clear example of such folding exists on the NE side of the duplex (Fig. 10c). These folds occur in the extensional sector of the instantaneous strain ellipse for dextral shear (Fig. 12a) and represent a classical example of quarter structures commonly seen on smaller scales (F in Fig. 11). There are also slightly oblique km-scale shear bands within the shear zone that, together with the foliation, create large-scale S-C' structures (Fig. 10a). Also, large asymmetric lenses that bear similarities to asymmetric porphyroclasts can be seen from the aeromagnetic images (Fig. 10b; c.f. Harris and Bédard, 2014 and Harris, this volume).

4.2.3. *Shear strain and displacement*

As for the Pernambuco shear zone, rotation of foliation in the wall rock into the shear zone can be used to constrain displacement. We have performed such analyses across three profiles (Fig. 9d). The western one (Profile A) captures the shear strain immediately west of the Seridó belt. A gradual increase in shear strain is recorded across the northern margin over a distance of about 12 km, adding up to a displacement of ~170 km before entering the core of the shear zone. In the core, where the average shear strain is roughly estimated to around 50–60 (Fig. 9d), the foliation is subparallel to the shear zone and affected by low-angle C' shear bands, which makes shear strain estimation inaccurate. As for the Pernambuco sections above, we could take the shear zone in the core to be similar to that of the most sheared part of the margin. This assumption, together with the ~17 km thickness of the zone, would imply around 1000 km of displacement. However, this must be an overestimate, because kinematically, the southern part of the Patos shear zone is sinistral, representing the northern part of NE-striking sinistral shear zones of the

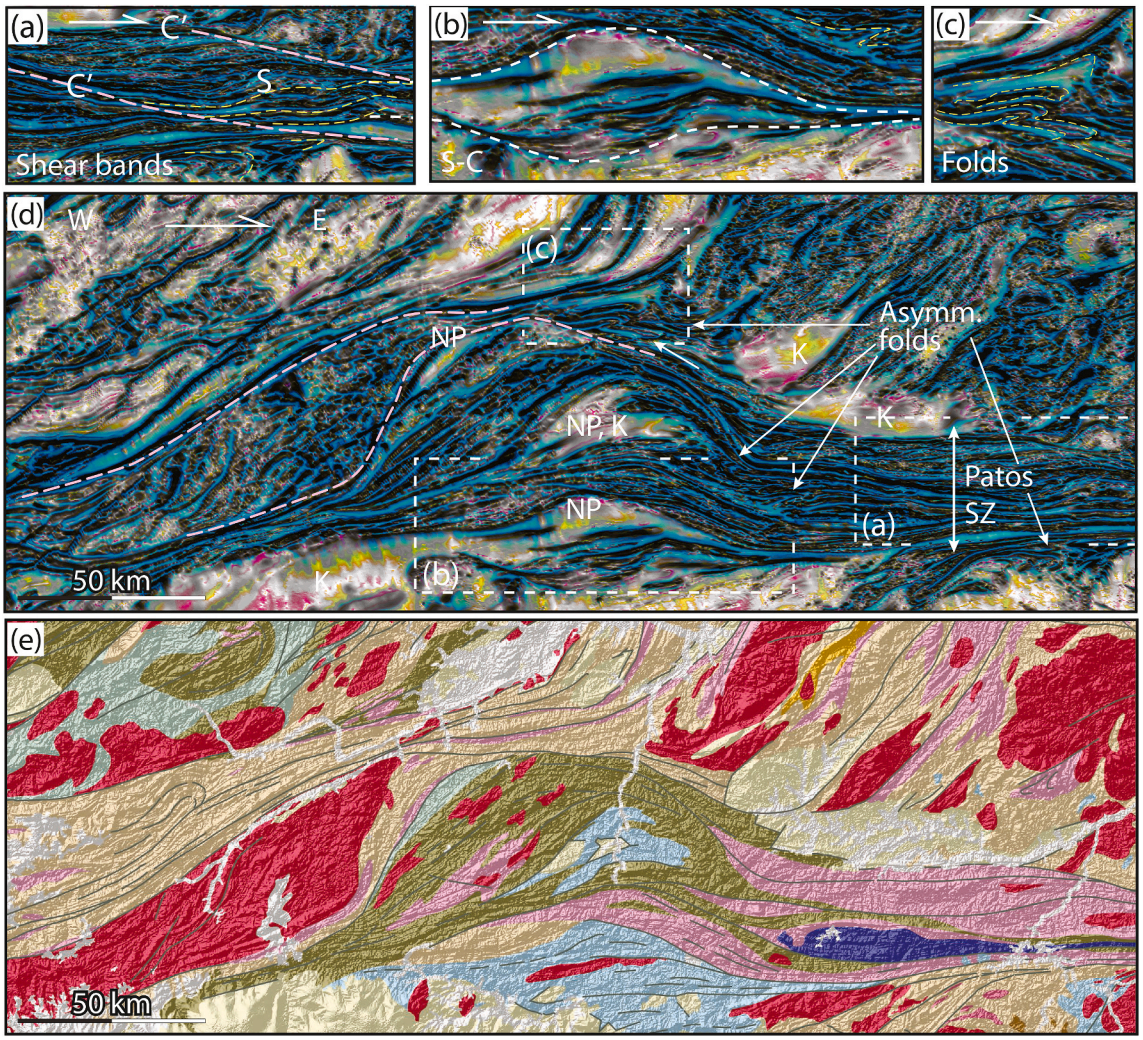

Fig. 10. The strike-slip duplex of the Patos shear zone as expressed by details from the magnetic anomaly map from Fig. 2e (a-d) and the geologic map with structural interpretation derived from the magnetic anomaly map. (a) km-scale S-C structure in the Patos shear zone east of the duplex. (b) sigmoidal structure at the base of the duplex. (c) asymmetric folds in the extensional sector of the duplex. (d) magnetic anomaly map with locations of a-c, (e) Geologic map and structural interpretation based on (d). See Fig. 2a for legend. All structures are consistent with dextral shear.

Central Domain that were zipped together with the dextral Patos during shearing.

The other two profiles show similar marginal geometry and strain and suggest similar levels of shear strain (γ close to 60) and minimum horizontal displacements of roughly 300 km (Profile B) and 200 km (Profile C). The eastward reduction in displacement estimates for profiles B and C goes together with an eastward reduction in thickness, which again is related to the bifurcation of the Patos shear zone immediately east of Profile A. A considerable part of the Patos shear zone strain is probably taken up by the Seridó belt, as documented as a dextral transpressional zone by several authors (e.g., Corsini et al., 1991; Hackspacher et al., 1997; Archanjo et al., 2002, 2013; Cioffi et al., 2021). This belt represents an eastward dextral splay of the shear zone. As such, it is different from the apparent splays seen along the Pernambuco shear zone, where the NE-SW splays themselves are sinistral (see below). Hence, we conclude that the main Patos shear zone involves displacement on the order of several hundred kilometers, and that this displacement is partitioned between northeastward-trending shear zones within and parallel to the Seridó belt and the eastward direct continuation of the Patos shear zone toward the Atlantic coast.

Displacement can be independently evaluated by the offset of lithologic units. Dextral shearing of the Edicarian Seridó Formation (Fig. 8a) implies more than 230 km of displacement in the northern margin and central part of the Patos shear zone. Along the southern margin, other Edicarian supracrustals are sheared at least 100 km. Adding these two components gives a minimum displacement estimate of 330 km for the Patos shear zone as a whole. Similarly, a minimum of 350 km displacement is indicated by sheared Archean units (notably the Granjeiro Complex; Archanjo et al., 2021) (Fig. 8c). Deflection of Tonian supracrustals indicates at least 120 km displacement along the south side of the East Patos shear zone (Fig. 8a). Paleoproterozoic metaigneous rocks within the Patos shear zone may also suggest displacement on the order of 350 km (Fig. 8b). Hence, the estimates from structural analysis and the distribution of lithologic units as observed from the geologic map pattern roughly agree, with a displacement of around 350 km, and a displacement of >100 km for the eastern segment that continues straight eastward to the Atlantic coast.

Finally, displacement can also be constrained from shear zone thickness, as thickness generally scales with displacement. Displacement was estimated for twelve shear zones (excluding the Pernambuco and Patos) using patterns of rotation of structures through the zones or the offset of lithologies and magnetically distinct anomalies. With a 10–72 km range in maximum displacement and a 2.5–20 km range in maximum thickness (Fig. 13) the data confirms that displacement scales positively and linearly with thickness, so that displacement for a given shear zone is close to 10 times its thickness. Our Borborema observations

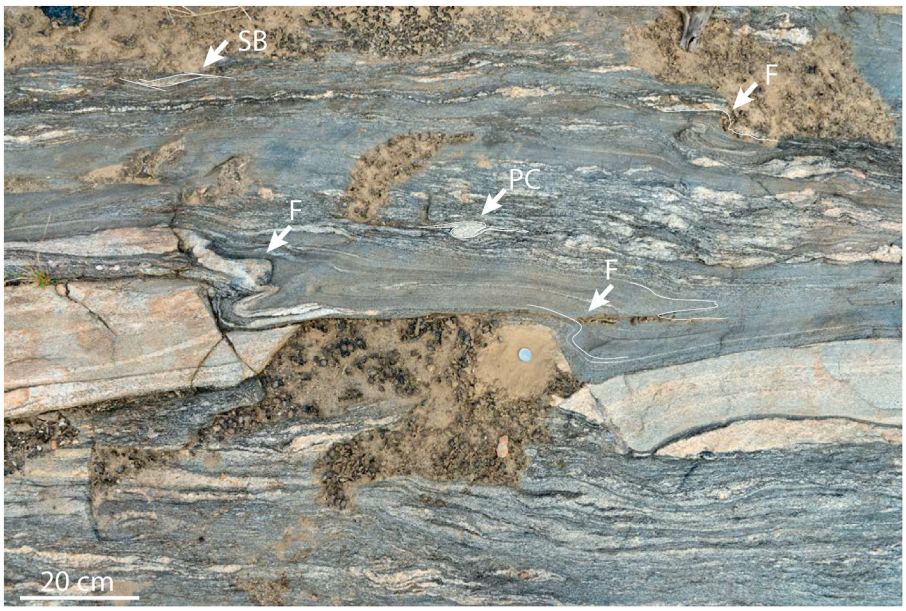

Fig. 11. Field example of kinematic indicators observable in the dextral Patos shear zone. F; asymmetric shear-related folds, several formed around boudinage corners. SB: shear bands. PC, asymmetric porphyroclasts (delta-type). Asymmetric boudinage of felsic layer also consistent with dextral sense of shear. Note the similarity between the fold at the boudinage corner (F) and the large-scale example of Fig. 10c. Location shown in Fig. 9.

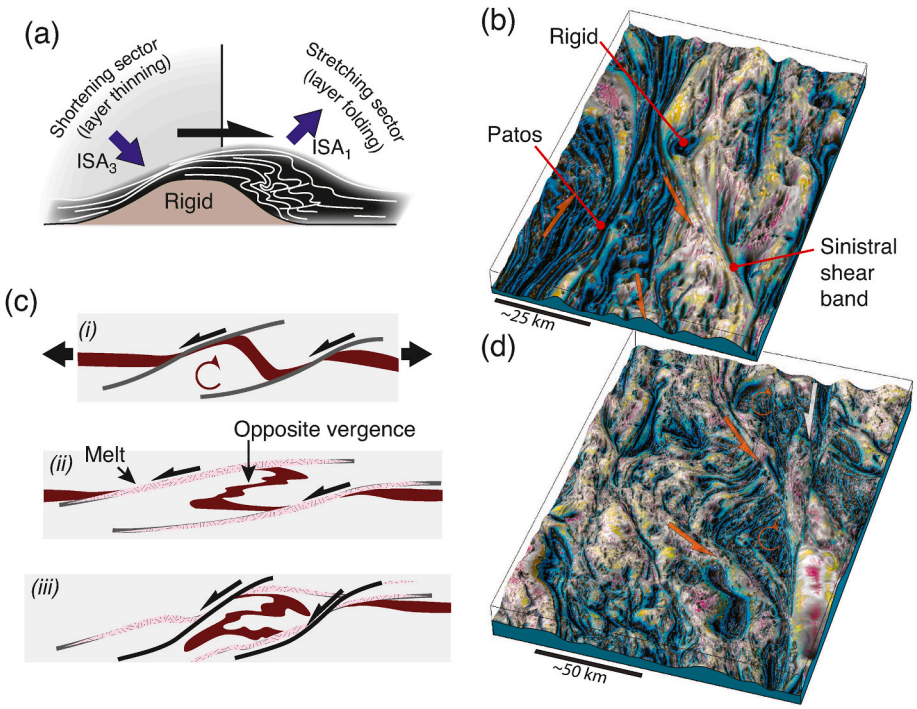

Fig. 12. (a) Formation of asymmetric folds around geometric irregularities (modified from Fossen and Cavalcante, 2017). ISA_1 and ISA_3 are the maximum and minimum instantaneous stretching axes, respectively. (b) Shear-band type structures in the Central domain south of the Patos shear zone, and a porphyroblast-style structure developed around a rigid granitic body. (c) Formation of back-rotated domains between shear bands (from Harris et al., 2002). (d) Two back-rotated domains bounded by shear bands, north of the Pernambuco shear zone. (b) and (d) are 3D perspective images based on a color-modified ternary image (Fig. 3f). (For interpretation of the references to color in this figure legend, the reader is referred to the Web version of this article.)

are consistent with the global trend presented by Fossen and Cavalcante (2017). When plotting our 200 km estimate from the Pernambuco and 350 km estimate from the Patos shear zone in Fig. 13, it is clear that they fit the trend defined by the other Borborema shear zones.

4.3. The shear zone network of the Central Domain

The Central (or Transverse) Domain is the volume of rocks bounded by the Patos and Pernambuco shear zones. This 200 km wide domain exposed in Borborema for 700 km is affected by a number of interconnected steep shear zones, each with a thickness of up to 20 km. Its numerous Neoproterozoic granites also show an average NE-SW oriented long axis (X-strain axis) that is different from that of the Northern Domain (closer to NNE-SSW), reflecting the difference in strain in these two domains (Fig. 2). This defines a structural expression that is different from the northern and, in particular, the southern domain, suggesting that these shear zones formed during the ductile shearing on the Patos and Pernambuco shear zones.

Based on our structural analysis of aeromagnetic anomaly images, the internal shear zones of the Central Domain fall into two populations that can be separated based on both orientation and kinematics (Fig. 2c). The dominant group is NE-SW oriented (average strike of 050 ± 2°) and

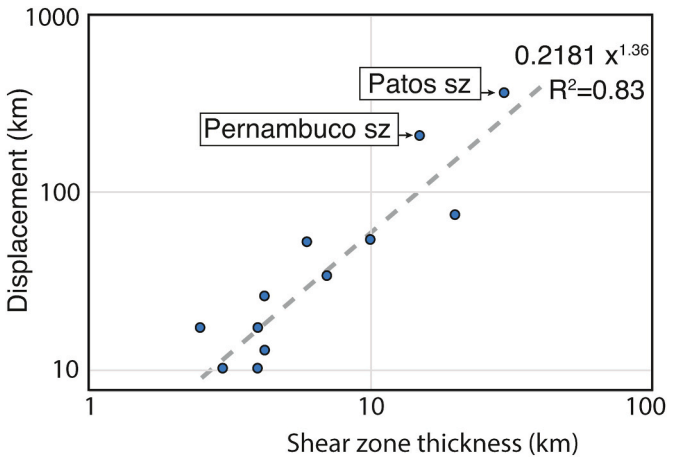

Fig. 13. Displacement plotted against thickness for shear zone in the Borborema region, mostly from the Central Domain. The Pernambuco shear zone is plotted with a thickness of 20 km and a displacement of 200 km, and the Patos with a displacement of 350 km.

sinistral, and thus antithetic to the other, dextral population (average strike of 100 ± 4°). The most prominent shear zone belonging to the dextral population is the Coxixola shear zone (Fig. 2c), which stretches for about 300 km in the eastern and central part of the Central Domain (Hollanda et al., 2010).

Different models can be called for to explain the internal shear zone pattern of the Central Domain. First of all, the prominent NE-SW trending set parallels the general lithologic structure of the domain, and if this map-scale lithologic zonation is pre-shearing, as indicated by Ganade de Araujo et al. (2014), this may explain why there are so many NE-SW trending shear zones in the Central Domain. One approach is to consider the two sets as extensional shear bands. The dextral set has a few elements that would classify as reverse shear bands (Dennis and Secor, 1990) and some are parallel to the Patos shear zone (C-bands), but most are slightly oblique to the Patos shear zone in an extensional sense, and can be classified as (extensional) C′ shear bands (e.g., Berthé et al., 1979) or ecc1 (Platt, 1984). The sinistral antithetic set would then be considered conjugate C″ shear bands or ecc2 (Platt, 1984; Xypolias, 2010). Well-developed C″ bands characterize shear zones with a coaxial component (e.g., subsimple shear or transpression), implying a component of N-S shortening across the system. Based primarily on numerical modeling, Grasemann et al. (2003) concluded that conjugate sets of shear bands indicate pure shear-dominated flow with a kinematic vorticity number Wk < 0.6, and Xypolias et al. (2010) used this approach to map variations in vorticity in ductile thrust zones in Greece. Xypolias (2010) also pointed out that shear bands can be used to calculate vorticity, as shown in his Fig. 11. Using this rather uncertain approach, the maximum angle of our synthetic set (30°) to the Patos shear zone would give a Wk of roughly 0.5 for the bulk deformation of the Central Domain (note that individual shear zones would still be approximately simple shear).

On the contrary, Finch et al. (2020) demonstrate numerically that subordinate antithetic shears can develop also during bulk simple shearing, particularly in models with a large (45%) weak phase. In the case of the Borborema, partial melt could possibly represent the weak phase, as seen in other migmatitic terrains (e.g., Cleven et al., 2020). If so, the deformation may be less coaxial than the above estimate of Wk ≈ 0.5. On the other hand, the antithetic shear bands reported by Finch et al. (2020) are very short, rather diffuse and not comparable to the extensive NE-striking shear zones of the Central Domain that are localized along lithostratigraphic domains.

In anisotropic rocks and analogue materials, antithetic shears may also be associated with boudinage of a competent layer (e.g., Lister and Snoke, 1984) or develop within a layer, forming a conjugate set with shear zones of the opposite sense of displacement due to strain partitioning during layer parallel slip (Harris and Cobbold, 1984).

As an alternative approach, we consider the two sets of semi-regional shear zones within the Central Domain as classical conjugate shear zones that initially were bisected by the instantaneous shortening direction. Any noncoaxial component would cause progressive rotation of the sets, and the bisector would not accurately represent the finite shortening direction anymore. In our case the antithetic set would rotate faster (clockwise) by an amount that increases with increasing W_k. The current angle between the bisectrix is only 15° west of north, making a $\theta = 75°$ to an E-W shear plane. Back-rotating the sinistral set counterclockwise would lower this angle, but the 60° counterclockwise rotation required for a simple shear deformation is unrealistic. Hence, although we do not know the exact rotation of this set, this approach implies a component of coaxial deformation that thinned and extended the Central Domain.

Based on the above considerations, we find indications of a component of N-S shortening across (and E-W stretching of) the Central Domain, and a roughly NNW shortening direction. This agrees with the interpretation by Archanjo et al. (2008), who pointed out the strong pure shear (N-S shortening) seen in the northern part of the Central Domain ESE of the town of Patos (Fig. 2c). It also agrees with shear zone data presented by Neves et al. (2012) from the SE Central Domain. Furthermore, several minor thrusts have been mapped and although their ages are not well constrained, they may be an expression of Neoproterozoic shortening (e.g., Neves et al., 2012; Silva and Neves, 2021). Regardless of the interpretation of the thrust, it is clear that the structural pattern observed in the Central Domain is different from the pattern north of the Patos shear zone, meaning that different domains accommodated strain in different ways.

4.4. The Northern Domain

The aeromagnetic images show a more complex picture north of the Patos shear zone, and location and kinematics of shear zones are not as easily defined as in the Central Domain. This domain shows an overall NNE-SSW trend of fabrics and lithologic contacts, with a variation in planar structures from steep to low-angle. Field observations show that steep shear zones are strike-slip dominated, while there are also low-angle shear zones interpreted as thrusts or extensional shear zones (Archanjo et al., 2002). There are also basement domes that may have resulted from extensive partial melting in the Neoproterozoic, and extensional shear zones may be related to this doming process. Hence, we have supported the aeromagnetic image interpretation with field observations when compiling the shear zone map shown in Fig. 2c. This map shows multiple NNE-striking dextral shear zones and an additional conjugate NNW-striking set of sinistral zones. Kinematic criteria involved include numerous kinematic indicators such as porphyroclast systems, veins, shear bands and boudins, and map-scale asymmetric shape of syntectonic granite plutons (e.g., Archanjo and Bouchez, 1991; Trindade et al., 1999; Archanjo et al., 2002; Souza et al., 2006; Archanjo et al., 2008).

5. Discussion and conclusions

5.1. Shear zone geometry, displacement and kinematics

This study shows how interpretations of different enhancements of aeromagnetic data not commonly used by structural geology researchers (although more common in the mineral exploration industry), and enhanced pseudo-gravity data (derived from the same original aeromagnetic data), may be integrated to provide a wealth of additional structural information that complements field mapping of the Borborema shear system in NE Brazil. In addition to identifying or confirming shear zones and confidentially constraining their shear sense (particularly successful in the Central Domain), regional tight to isoclinal folds are identified in the Northern Domain using edge enhanced pseudo-

gravity images (which are shown to be invaluable in defining deep domain boundaries and their geometry), where only a few minor folds appear in aeromagnetic images enhancing the upper crust. This interpretation is consistent with field observations of NNE-SSW striking dextral shear zones and thrusts (Fig. 2c). Aeromagnetic images portray spectacular examples of the range of fold styles, reorientation and superposition, producing a full spectrum of fold interference patterns establish by Ramsay (1967) at a regional scale similar to those observed at the outcrop and thin section scales, and produced in physical and numerical simulations (e.g., Grasemann et al., 2004).

The analyses presented here are consistent with an interpretation of the Patos-Pernambuco shear zone system as an enormous intracontinental dextral transcurrent shear system, where the exposed level developed at mid-crustal depths. We have employed classical shear zone theory to estimate the kinematics and strains related to the shear zones and find a consistent pattern of both dextral and sinistral zones. The Patos and Pernambuco shear zones show evidence of very high shear strains and accumulated lateral dextral offsets on the order of 200 and 350 km, respectively. These shear zones themselves must therefore be close to simple shear, as confirmed by very consistent asymmetry of internal shear zone structures. However, the domains between and outside of these two major shear zones show a different deformation style with two sets of conjugate shear zones.

A particularly interesting feature in this respect is the many NE-striking sinistral antithetic shear zones in the Central Domain, and similarly oriented shear zones in the Northern Domain with opposite (dextral) kinematics. This alone implies a change in strain regime across the Patos shear zone. In the Northern Domain, field-based kinematic indicators show a combination of NE-striking dextral shear zones accompanied by N to NNW-striking sinistral shear zones (Fig. 2c), and together they indicate an ENE-WSW apparent shortening direction that is very different from that of the Central Domain (see rose diagrams in Fig. 2c). The orientations of these internal shear zones do not fit those of typical shear bands (C, C′ or C″) and suggest an influence of coaxial strain. The Southern Domain (south of the Pernambuco shear zone) also show shear zones with kinematics and orientations in agreement with a component of N-S shortening, similar to the Central Domain. We suggest from these observations that the Neoproterozoic deformation in the Borborema Province is participated into simple shear localized on the two major shear zones and more complex and overall lower vorticity-type deformation of a nature that differs between the Central and Northern domains.

To better constrain this strain partitioning and the deformation in general in the Borborema region, dating of individual shear zones is necessary. It is unlikely that all shear zones were active at the same time everywhere, and it is also unlikely that the far-field kinematic boundary conditions were stable over the ca. 50 million years of dextral shearing in this region. More work could also be done on constraining the pre-shearing rheologic structure, including the rift-related structures and how they influence the development of the Borborema shear zone system.

5.2. Tectonic implications

Altogether, following peak metamorphism between 650 and 590 Ma in the Central Domain Neves et al., 2015), more than 550 km of combined dextral shear is indicated during the Ediacaran. Based on AMS studies and radiometric dating, synkinematic plutons were emplaced between 585 and 571 Ma (Archanjo et al., 2998, 2013; Hollanda et al., 2010; Ávila et al., 2020). Shearing appears to have peaked at around 590-560 Ma, but locally lasted into the Cambrian (Hollanda et al., 2010; Cioffi et al., 2021) when brittle reactivation resulted in the formation of pull-apart basins in which molasse sediments were deposited (Ávila et al., 2020). Regionally the Brasiliano orogeny initiated with continental collisions around 640-630 Ma, following a prolonged period of rifting (Neves et al., 2015). The interpretation that the Pernambuco shear zone represents a reactivated rift boundary of such an Early Tonian pre-Brasiliano rift system (Neves et al., 2020) is supported by the total field pseudo-gravity image in Fig. 4a that is dominated by deep crustal features that may equate to rift margins. That this may also be the case for the Patos shear zone (Neves, 2018) is supported by the same pseudogravity image, and the continuity of some units from the Southern to Northern domains places doubt on the suture model presented for this structure (Brito Neves et al., 2016). In general, a model where the shear zones formed in response to Brasiliano–Pan-African shortening of a rifted hot crust (Ganade et al., 2021) seems likely. Our observations fit the widely accepted model of lateral dextral shear primarily driven by an eastward push from the Amazon craton (Archanjo et al., 2021).

Our structural interpretation shows that the Patos and Pernambuco shear zones accumulated approximately 350 and 200 km of lateral offset, respectively, through simple shear-dominated deformation, amounting to a total of ca. 550 km of lateral displacement between the Northern and Southern domains. In addition, the different domains that are delimited by the major shear zones deformed in different ways, reflecting complex deformation partitioning at the 100-km scale. The difference in deformation between the Central and Northern domains suggest a more complex deformation pattern than the rotational extrusion model presented by Ganade de Araujo et al. (2014b), who also assign an undocumented sinistral movement to the NNE-striking dextral shear zones in the Northern Domain west of the Seridó belt to fit their model (their Fig. 4). Although more work is needed to better understand the strain patterns portrayed in this work, particularly through dating of shear zone activity in this complex shear zone array, we have shown how aeromagnetic data can contribute to map and interpret the Neoproterozoic deformation of this and similar regions of variable ductile crustal deformation.

CRediT authorship contribution statement

Haakon Fossen: Conceptualization, Investigation, Visualization, Writing – original draft, Writing – review & editing. **Lyal B. Harris:** Conceptualization, Investigation, Methodology, Data curation, Verification. **Carolina Cavalcante:** Investigation, Writing – review & editing. **Carlos José Archanjo:** Writing – review & editing. **Carlos F. Ávila:** Writing – review & editing.

Declaration of competing interest

The authors declare that they have no known competing financial interests or personal relationships that could have appeared to influence the work reported in this paper.

Acknowledgments

Aeromagnetic and gravity data processed by LH using Seequent's Oasis Montaj and software by P. Keating (NRCan, retired) forms part of research funded by Ero Copper Corporation, who provided original, unfiltered aeromagnetic data and is thanked for permission to publish the derived images in this article, but played no direct role in the research presented herein. CJA and CA acknowledge the Fundação de Amparo à Pesquisa do Estado de São Paulo (FAPESP), CJA the support of the Brazilian agencies CAPES and CNPq (grant 304979/20016-3) and CC thanks CNPq for support through project number 434202/2018-5. LH acknowledges the understanding and appreciation of structural geology gained from field trips and discussions with John Ramsay whilst a student and instructor at Rennes University, France, that left lasting impressions. We are thankful for constructive comments by Francisco Hilario Bezerra and two unknown reviewers that helped improve the text.

Appendix A. Supplementary data

Supplementary data to this article can be found online at https://doi.org/10.1016/j.jsg.2022.104573.

References

Archanjo, C.J., Bouchez, J.-L., 1991. Le Serido, une chaîne transpressive dextre au Protérozoïque supérieur du Nord-Est du Brésil. Bull. Soc. Géol. France 162, 637–647.

Archanjo, C.J., Silva, E.R., Caby, R., 1999. Magnetic fabric and pluton emplacement in a transpressive shear zone system: the Itaporanga porphyritic granitic pluton (northeast Brazil). Tectonophysics 312, 331–345.

Archanjo, C.J., Trindade, R., Bouchez, J.-L., Ernesto, M., 2002. Granite fabrics and regional-scale strain partitioning in the Seridó belt (Borborema Province, NE Brazil). Tectonics 21, 14.

Archanjo, C.J., Hollanda, M.H.B.M., Rodrigues, S.W.O., Neves, B.B.B., Armstrong, R., 2008. Fabrics of pre- and syntectonic granite plutons and chronology of shear zones in the Eastern Borborema Province, NE Brazil. J. Struct. Geol. 30, 310–326.

Archanjo, C.J., Viegas, G., de Hollanda, M.H.B.M., 2013. Timing of the HT/LP transpression in the neoproterozoic Seridó belt (Borborema province, Brazil): constraints from U\Pb (SHRIMP) geochronology and implications for the connections between NE Brazil and west Africa. Gondwana Res. 23, 701–714.

Archanjo, C.J., Hollanda, M.H.B.M., Viegas, L.G.F., 2021. Late Ediacaran lateral-escape tectonics as recorded by the Patos shear zone (Borborema Province, NE Brazil). Braz. J. Geol. 51 https://doi.org/10.1590/2317-4889202120200132.

Arthaud, M.H., Caby, R., Fuck, R.A., Dantas, E.L., Parente, C.V., 2008. Geology of the Northern Borborema Province, NE Brazil and its Correlation with Nigeria, NW Africa, vol. 294. Geological Society, London, Special Publications, Geological Society, London, Special Publications, pp. 49–67.

Ávila, C.F., Archanjo, C.J., Fossen, H., Hollanda, M.H.B.M., 2019. Zippered shear zone model for interacting shear zones in the Borborema Province, Brazil, as constrained by U-Pb dating. Tectonics. https://doi.org/10.1029/2019TC005547.

Ávila, C.F., Archanjo, C.J., Hollanda, M.H.B.M., Macêdo Filhoa, A., Lemos-Santosa, D.V., 2020. Shear zone cooling and fabrics of synkinematic plutons evidence timing and rates of orogenic exhumation in the northwest Borborema Province (NE Brazil). Precambrian Res. 350 https://doi.org/10.1016/j.precamres.2020.105940.

Baranov, V., 1957. A new method for interpretation of aeromagnetic maps: pseudo-gravimetric anomalies. Geophysics 22, 359–383.

Berthé, D., Choukroune, P., Gapais, D., 1979. Orientations preferentielles du quartz et orthogneissification progresive en regime cisaillement: L'exemple du cisaillement sudaroricain. Bull. Mineral. 102, 265–272.

Bezerra, F.H.R., Rossetti, D.F., Oliveira, R.G., Medeiros, W.E., Neves, B.B.B., Balsamo, F., Nogueira, F.C.C., Dantas, E.L., Andrades Filho, C., Góes, A.M., 2014. Neotectonic reactivation of shear zones and implications for faulting style and geometry in the continental margin of NE Brazil. Tectonophysics 614, 78–90.

Brito Neves, B.B., Santos, E.J.d., Fuck, R.A., Santos, L.C.M.L., 2016. A preserved early Ediacaran magmatic arc at the northernmost portion of the Transversal Zone central subprovince of the Borborema Province, Northeastern South America. Braz. J. Geol. 46, 491–508.

Caby, R., 1989. Precambrian Terranes of Benin-Nigeria and Northeast Brazil and the Late Proterozoic South Atlantic Fit, vol. 230. Geological Society of America Special Paper, pp. 145–158.

Caby, R., Arthaud, M.H., Archanho, C.J., 1995. Lithostratigraphy and petrostructural characterization of supracrustal units in the Brasiliano Belt of Northeast Brazil: geodynamic implications. J. S. Am. Earth Sci. 8, 235–246.

Caby, R., Atthaud, M., 1986. Major Precambrian nappes of the Brazilian belt, Ceará, northeast Brazil. Geology 14, 871–874.

Carreras, J., Cosgrove, J.W., Druguet, E., 2013. Strain partitioning in banded and/or anisotropic rocks: implications for inferring tectonic regimes. J. Struct. Geol. 50, 7–21.

Castellan, P., Viegas, G., Faleiros, F.M., 2020. Brittle–ductile fabrics and P–T conditions of deformation in the East Pernambuco shear zone (Borborema Province, NE Brazil). J. Geol. Soc. 178 https://doi.org/10.1144/jgs2020-109.

Cavalcante, G.C.G., Viegas, G., Archanjo, C.J., da Silva, M.E., 2016. The influence of partial melting and melt migration on the rheology of the continental crust. J. Geodyn. 101, 186–199. https://doi.org/10.1016/j.jog.2016.06.002.

Caxito, F., Uhlein, A., Stevenson, R., Uhlein, G.J., 2014. Neoproterozoic oceanic crust remnants in northeast Brazil. Geology 42, 387–390.

Caxito, F.A., Uhlein, A., Dantas, E.L., Stevenson, R., Salgado, S.S., Dussin, I.A., Sial, A.d. N., 2016. A complete Wilson cycle recorded within the Riacho do Pontal orogen, NE Brazil: implications for the neoproterozoic evolution of the Borborema province at the heart of West Gondwana. Precambrian Res. 282, 97–120. https://doi.org/10.1016/j.precamres.2016.07.001.

Caxito, F.A., Uhlein, A., Dantas, E., Stevenson, R., Egydio-Silva, M., Salgado, S.S., 2017. The Rio Preto and Riacho Do Pontal Belts, pp. 221–239. https://doi.org/10.1007/978-3-319-01715-0_12.

Caxito, F.d.A., Santos, L.C.M.d.L., Ganade, C.E., Bendaoud, A., Fettous, E.-H., Bouyo, M. H., 2020. Toward an integrated model of geological evolution for NE Brazil-NW Africa: the Borborema Province and its connections to the Trans-Saharan (Benino-Nigerian and Tuareg shields) and Central African orogens. Braz. J. Geol. 50 https://doi.org/10.1590/2317-4889202020190122.

Caxito, F.A., Basto, C.F., Santos, L.C.M.d.L., Dantas, E.L., Medeiros, V.C.d., Dias, T.G., Barrote, V., Hagemann, S., Alkmim, A.R., Lana, C., 2021. Neoproterozoic magmatic arc volcanism in the Borborema Province, NE Brazil: possible flare-ups and lulls and implications for western Gondwana assembly. Gondwana Res. 92, 1–25. https://doi.org/10.1016/j.gr.2020.11.015.

Cioffi, C.R., Meira, V.T., Trindade, R.I.F., Lanari, P., Ganade de Araujo, C.E., Gerdes, A., 2021. Long-lived intracontinental deformation associated with high geothermal gradients in the Seridó Belt (Borborema Province, Brazil). Precambrian Res. 358 https://doi.org/10.1016/j.precamres.2021.106141.

Clegg, P., Holdsworth, R.E., 2005. Complex deformation as a result of strain partitioning in transpression zones: an example from the Leinster Terrane, SE Ireland. J. Geol. Soc. 162, 187–202.

Cleven, N.R., Harris, L.B., Guilmette, C., 2020. Structural Interpretation Of Enhanced High-Resolution Aeromagnetic Depth Slices Of The Eeyou Istchee Baie-James Region, Québec Superior Province. MB 2020-02, MERN, Québec. https://gq.mines.gouv.qc.ca/documents/EXAMINE/MB202002/MB202002RAP001.pdf.

Cooper, G.R.J., Cowan, D.R., 2005. Differential reduction to the pole. Comput. Geosci. 31, 989–999.

Corsini, M., Vauchez, A., Archanjo, C., Jardim de, Sá, 1991. Strain transfer at continental scale from a transcurrent shear zone to a transpressional belt: the Patos-Seridó system, northeastern Brazil. Geology 19, 586–589.

Corsini, M., Vauchez, A., Caby, R., 1996. Ductile duplexing at a bend of a continental-scale strike-slip shear zone: example from NE Brazil. J. Struct. Geol. 18, 385–394.

Coward, M.P., 1976. Strain within ductile shear zones. Tectonophysics 34, 181–197.

Coward, M.P., Kim, J.H., 1981. Strain within thrust sheets. In: McClay, K.R.P., Price, N.J. (Eds.), Thrust and Nappe Tectonics, vol. 9. Geological Society, London, Special Publications, pp. 275–292.

de Castro, D.L., Bezerra, F.H., Fuck, R.A., Vidotti, R.M., 2016. Geophysical evidence of pre-sag rifting and post-rifting fault reactivation in the Parnaíba basin, Brazil. Solid Earth 7, 529–548.

de Paula Garcia, P.M., Carrilho, E.L.V., Ribeiro, B.P., Misi, A., Sá, J.H.d.S., Rios, D.C., 2021. Geology, petrogenesis, and geochronology of the Rio Salitre complex: implications for the Paleoproterozoic evolution of the northern São Francisco craton, Brazil. J. S. Am. Earth Sci. 107 https://doi.org/10.1016/j.jsames.2020.103112.

de Wit, M.J. Stankiewicz J., Reeves, C., 2008. Restoring Pan-African-Brasiliano Connections: More Gondwana Control, Less Trans-Atlantic Corruption, vol. 294. Geological Society, London, Special Publications, pp. 399–412.

Dennis, A.J., Secor, D.T., 1990. On resolving shear direction in foliated rocks deformed by simple shear. Geol. Soc. Am. Bull. 102, 1257–1267.

Dentith, M., Mudge, S.T., 2014. Geophysics for the Mineral Exploration Geoscientist. Cambridge University Press, p. 454.

Domingos, N.R.R., Medeiros, W.E., Oliveira, R.G., 2020. Geophysical evidence for doming during the Pan-African/Brasiliano orogeny in the Seridó belt, Borborema province, Brazil. Precambrian Res. 350 https://doi.org/10.1016/j.precamres.2020.105870.

Escher, A., Escher, J.C., Watterson, J., 1975. The reorientation of the Kangâmiut dike Swarm, west Greenland. Can. J. Earth Sci. 12, 158–173.

Fetter, A.H., Santos, T.J.S., Van Schmus, W.R., Hackspacher, P.C., Brito Neves, B.B., Arthaud, M.H., Nogueira Neto, J.A., Wernick, E., 2003. Evidence for neoproterozoic continental arc magmatism in the Santa Quitéria batholith of Ceará state, NW Borborema province, NE Brazil: implications for assembly of West Gondwana. Gondwana Res. 6, 265–273.

Finch, M.A., Bons, P.D., Steinbach, F., Grier, A., Llorens, M.-G., Gomez-Rivas, E., Ran, H., de Riese, T., 2020. The ephemeral development of C′ shear bands: a numerical modelling approach. J. Struct. Geol. 139 https://doi.org/10.1016/j.jsg.2020.104091.

Fossen, H., 2016. Structural Geology, second ed. Cambridge University Press.

Fossen, H., Cavalcante, G.C.G., 2017. Shear zones - a review. Earth Sci. Rev. 171, 434–455.

Fossen, H., Tikoff, B., 1993. The deformation matrix for simultaneous simple shearing, pure shearing, and volume change, and its application to transpression/transtension tectonics. J. Struct. Geol. 15, 413–422.

Fossen, H., Tikoff, B., 1998. Extended models of transpression/transtension and application to tectonic settings. In: Holdsworth, R.E., Strachan, R.A., Dewey, J.F. (Eds.), Continental Transpressional and Transtensional Tectonics. Geol. Soc. Lon. Spec. Publ., pp. 15–33

Ganade de Araujo, C.E., Rubatto, D., Hermann, J., Cordani, U.G., Caby, R., Basei, M.A., 2014a. Ediacaran 2,500-km-long synchronous deep continental subduction in the West Gondwana Orogen. Nat. Commun. 5, 5198. https://doi.org/10.1038/ncomms6198.

Ganade de Araujo, C.E., Weinberg, R.F., Cordani, U.G., 2014b. Extruding the Borborema province (NE-Brazil): a two-stage neoproterozoic collision process. Terra. Nova 26, 157–168. https://doi.org/10.1111/ter.12084.

Ganade, C.E., Weinberg, R.F., Caxito, F.A., Lopes, L.B.L., Tesser, L.R., Costa, I.S., 2021. Decratonization by rifting enables orogenic reworking and transcurrent dispersal of old terranes in NE Brazil. Sci. Rep. 11, 5719.

Grasemann, B., Stüwe, K., Vannay, J.-C., 2003. Sense and non-sense of shear in flanking structures. J. Struct. Geol. 25, 19–34.

Grasemann, B., Wiesmayr, G., Draganits, E., Fusseis, F., 2004. Classification of refold structures. J. Geol. 112, 119–125. https://doi.org/10.1086/379696.

Hackspacher, P.C., Dantas, E., Neves, B.B.B., Legrand, J.M., 1997. Northwestern overthrusting and related lateral escape during the Brasiliano orogeny north of the Patos lineament, Borborema province, Northeast Brazil. Int. Geol. Rev. 39, 609–620.

Harris, L.B., This volume. Folding and fracturing of rocks — interpretations at different crustal depths using enhanced aeromagnetic and gravity data. J. Struct. Geol.,.

Harris, L.B., Bédard, J.H., 2014. Crustal evolution and deformation in a non-plate tectonic Archaean Earth: comparisons with venus. In: Dilek, Y., Furnes, H. (Eds.), Evolution of Archean Crust and Early Life, Modern Approaches in Solid Earth

Sciences 7. Springer, pp. 215–288, 978-94-007-7614-2 & ISBN 978-94-007-7615-9 (eBook).
Harris, L.B., Cobbold, P.R., 1984. Development of conjugate shear bands during bulk simple shearing. J. Struct. Geol. 7, 37–44.
Harris, L.B., Koyi, H.A., Fossen, H., 2002. Mechanisms for folding of high-grade rocks in extensional tectonic settings. Earth Sci. Rev. 59, 163–210.
Holden, D., Archibald, N., Boschetti, F., Jessell, M.W., 2000. Inferring geological structures using wavelet-based multiscale edge analysis and forward models. Explor. Geophys. 31, 617–621.
Hollanda, M.H.B.M., Archanjo, C.J., Souza, L.C., Armstrong, R., Vasconcelos, P.M., 2010. Cambrian mafic to felsic magmatism and its connections with transcurrent shear zones of the Borborema Province (NE Brazil): implications for the late assembly of the West Gondwana. Precambrian Res. 178, 1–14.
Hornby, P., 2019. Potential Field Surveys, Analyses, And Interpretation For Cornell's Earth Source Heat Project [last consulted. https://ecommons.cornell.edu/bitstream/handle/1813/69612/Horowitz_report_2020.pdf?sequence=2andisAllowed=y. (Accessed August 2021).
Hornby, P., Boschetti, F., Horowitz, F.G., 1999. Analysis of potential field data in the wavelet domain. Geophys. J. Int. 137, 175–196.
Isles, D., Rankin, L., 2011. Geological Interpretation Of Aeromagnetic Data. ASEG. https://www.aseg.org.au/sites/default/files/ebook-ASEG-eBook-Geo-Interpretation-of-Aeromagnetic-Data-Opt-for-user-1621.pdf.
Jekeli, C., Erkan, K., Huang, O., 2010. Gravity vs pseudo-gravity: a comparison based on magnetic and gravity gradient measurements. In: Mertikas, S.P. (Ed.), Gravity, Geoid and Earth Observation. Springer Nature, pp. 123–127.
Jessell, M.W., Amponsah, P.O., Baratoux, L., Asiedu, D.K., Lohd, G.K., Ganne, J., 2012. Crustal-scale transcurrent shearing in the Paleoproterozoic Sefwi-Sunyani-Comoé region, West Africa. Precambrian Res. 212–213, 155–168.
Johnson, S.E., Lenferink, H.J., Marsh, J.H., Price, N.J., Koons, P.O., West, D.P., 2009. Kinematic vorticity analysis and evolving strength of mylonitic shear zones: new data and numerical results. Geology 37, 1075–1078.
Jones, R.R., Tanner, P.W.G., 1995. Strain partitioning in transpression zones. J. Struct. Geol. 17, 793–802.
Julios, E.A., Martial, F.E., Maurice, K., Jules, T.K., Cliff, C.K.S., Ludovic, A.M., 2020. Structural characterization of the Pan-African Ndieki area in the Foumban-Bankim shear zone (west Cameroon): constraints from field observations and microstructures. Arabian J. Geosci. 13, 831. https://doi.org/10.1007/s12517-020-05775-z.
Likkason, O.K., 2011. Spectral analysis of geophysical data. In: Chen, D.M. (Ed.), Advances in Data, Methods, Models and Their Applications in Geoscience. Intech Open, ISBN 978-953-307-737-6. https://doi.org/10.1016/j.tecto.2019.05.017. https://www.intechopen.com/chapters/25378.
Lister, G.S., Snoke, A.W., 1984. S-C mylonites. J. Struct. Geol. 6, 617–638.
Lister, G.S., Williams, P.F., 1983. The partitioning of deformation in flowing rock masses. Tectonophysics 92, 1–33.
Liu, S., Tommasi, A., Vauchez, A., Mazzucchelli, M., 2019. Crust-mantle coupling during continental convergence and break-up: constraints from peridotite xenoliths from the Borborema Province, northeast Brazil. Tectonophysics 766, 249–269.
Marques, F.O., Schmid, D.W., Andersen, T.B., 2007. Applications of inclusion behaviour models to a major shear zone system: the Nordfjord-Sogn detachment zone in western Norway. J. Struct. Geol. 29, 1622–1631.
Martelat, J.-E., Lardeaux, J.-M., Nicollet, C., Rakotondrazafy, R., 2000. Strain pattern and late Precambrian deformation history in southern Madagascar. Precambrian Res. 102, 1–20.
Melo, A.C.C., Lopes de Castro, D., Custódio de Oliveira, D., Bezerra Maia de Hollanda, M. H., 2022. Mesozoic dike swarms in Borborema Province (NE Brazil): a structural analysis based on airborne geophysical data and field work. J. S. Am. Earth Sci. 113.
Miller, H.G., Singh, V., 1994. Potential-field tilt - a new concept for location of potential-field sources. J. Appl. Geophys. 32, 213–217.
Miranda, T.S., Neves, S.P., Celestino, M.A.L., Roberts, N.M.W., 2020. Structural evolution of the Cruzeiro do Nordeste shear zone (NE Brazil): Brasiliano-Pan-African- ductile-to-brittle transition and Cretaceous brittle reactivation. J. Struct. Geol. 141 https://doi.org/10.1016/j.jsg.2020.104203.
Mocitaiba, L.S.R., Lopes de Castro, D., Custódio de Oliveira, D., 2017. Cartografia Geofísica Regional Do Magmatismo Mesozoico Na Bacia Do Parnaíba/Regional Geophysical Mapping of the Mesozoic Magmatism in the Parnaíba Basin, vol. 17. Revista do Instituto de Geociências, pp. 16–192.
Moreau, F., Gibert, D., Holschneider, M., Saracco, G., 1997. Wavelet analysis of potential fields. Inverse Probl. 13, 165–178. https://doi.org/10.1088/0266-5611/13/1/013.
Neves, S.P., 2018. Comment on "A preserved early Ediacaran magmatic arc at the northernmost part of the transversal zone - central domain of the Borborema Province, Northeast of South America". In: de Brito Neves, B.B., et al. (Eds.), Brazilian Journal of Geology, vol. 48, pp. 623–630, 2016.
Neves, S.P., Mariano, G., 1999. Assessing the tectonic significance of a large-scale transcurrent shear zone system: the Pernambuco lineament, northeastern Brazil, NE Brazil. J. Struct. Geol. 21, 1369–1383.
Neves, S.P., Vauchez, A., Feraud, G., 2000. Tectono-thermal evolution, magma emplacement, and shear zone development in the Caruaru area (Borborema Province, NE Brazil). Precambrian Res. 99, 1–32.
Neves, S.P., da Silva, J.M.R., Mariano, G., 2005. Oblique lineations in orthogneisses and supracrustal rocks: vertical partitioning of strain in a hot crust (eastern Borborema Province, NE Brazil). J. Struct. Geol. 27, 1513–1527. https://doi.org/10.1016/j.jsg.2005.02.002.
Neves, S.P., Bruguier, O., Vauchez, A., Bosch, D., da Silva, J.M.R., Mariano, G., 2006. Timing of crust formation, deposition of supracrustal sequences, and Transamazonian and Brasiliano metamorphism in the East Pernambuco belt (Borborema Province, NE Brazil): implications for western Gondwana assembly. Precambrian Res. 149, 197–216.
Neves, S.P., Monié, P., Bruguier, O., Rangel da Silva, J.M., 2012. Geochronological, thermochronological and thermobarometric constraints on deformation, magmatism and thermal regimes in eastern Borborema Province (NE Brazil). J. S. Am. Earth Sci. 38, 129–146.
Neves, S.P., Bruguier, O., da Silva, J.M.R., Mariano, G., da Silva Filho, A.F., Teixeira, C. M.L., 2015. From extension to shortening: dating the onset of the Brasiliano orogeny in eastern Borborema province (NE Brazil). J. S. Am. Earth Sci. 58, 238–256.
Neves, S.P., Rangel da Silva, J.M., Bruguier, O., 2016. The transition zone between the Pernambuco-Alagoas Domain and the Sergipano Belt (Borborema Province, NE Brazil): geochronological constraints on the ages of deposition, tectonic setting and metamorphism of metasedimentary rocks. J. S. Am. Earth Sci. 72, 266–278.
Neves, S.P., Bezerra, J.P.S., Bruguier, O., França, R.H.M., 2020. Evidence for Early Tonian (ca. 1000-940 Ma) continental rifting in southern Borborema Province (NE Brazil): tectonic inheritance and shear zone nucleation during assembly of West Gondwana. Int. Geol. Rev. 63, 851–865.
Neves, S.P., Tommasi, A., Vauchez, A., Carrino, T.A., Banerjee, S., 2021a. The Borborema strike-slip shear zone system (NE Brazil): large-scale intracontinental strain localization in a heterogeneous plate. Lithosphere. https://doi.org/10.2113/2021/6407232, 2021.
Neves, S.P., Teixeira, C.M.L., Bruguier, O., 2021b. 870-850 Ma-old magmatic event in eastern Borborema province, NE Brazil: another Tonian failed attempt to break up the São Francisco Paleoplate? J. S. Am. Earth Sci. 105 https://doi.org/10.1016/j.jsames.2020.102917.
Oliveira, R.G., Medeiros, W.E., 2018. Deep crustal framework of the Borborema Province, NE Brazil, derived from gravity and magnetic data. Precambrian Res. 315, 45–65.
Oliveira, E.P., Windley, B.F., Araújo, M.N.C., 2010. The Neoproterozoic Sergipano orogenic belt, NE Brazil: a complete plate tectonic cycle in western Gondwana. Precambrian Res. 181, 64–84.
Passchier, C.W., Simpson, C., 1986. Porphyroclast systems as kinematic indicators. J. Struct. Geol. 8, 831–843.
Pereira, L.C.L., Santos, L.C.M.d.L., Carrino, T.A., 2019. The role of airborne geophysics in the investigation of gold occurrences in the Itapetim Region, Borborema Province, Northeast Brazil. Braz. J. Geol. 49 https://doi.org/10.1590/2317-4889201920190028.
Platt, J.P., 1984. Secondary cleavages in ductile shear zones. J. Struct. Geol. 6, 439–442.
Poisson, S.D., 1826. Mémoire sur la théorie du magnétisme. Mémoir. Acad. Roy. Sci. Inst. France 5, 247–348.
Ramberg, H., 1975. Particle paths, displacement and progressive strain applicable to rocks. Tectonophysics 28, 1–37.
Ramberg, H., Ghosh, S.K., 1977. Rotation and strain of linear and planar structures in three-dimensional progressive deformation. Tectonophysics 40, 309–337.
Ramsay, J.G., 1967. Folding and Fracturing of Rocks. McGraw-Hill, New York.
Ramsay, J.G., 1980. Shear zone geometry: a review. J. Struct. Geol. 2, 83–99.
Ramsay, J.G., Allison, I., 1979. Structural analysis of shear zones in an alpinised Hercynian granite. Schweiz. Mineral. Petrogr. Mittil. 59, 251–279.
Ramsay, J.G., Graham, R.H., 1970. Strain variation in shear belts. Can. J. Earth Sci. 7, 786–813.
Ramsay, J.G., Huber, M.I., 1983. The Techniques of Modern Structural Geology: Strain Analysis. Academic Press, London.
Robin, P.-Y., Cruden, A.R., 1994. Strain and vorticity patterns in ideally ductile transpression zones. J. Struct. Geol. 16, 447–466.
Rocha, M.P., Azevedo, P.A.d., Assumpção, M., Pedrosa-Soares, A.C., Fuck, R., Von Huelsen, M.G., 2019. Delimiting the neoproterozoic São Francisco Paleocontinental block with P-wave traveltime tomography. Geophys. J. Int. 219, 633–644. https://doi.org/10.1093/gji/ggz323.
Roest, W., Verhoef, J., Pilkington, M., 1992. Magnetic interpretation using the 3-D analytic signal. Geophysics 57, 116–125.
Salem, A., Williams, S., Fairhead, D., Smith, R., Ravat, D., 2007. Interpretation of magnetic data using tilt-angle derivatives. Geophysics 78, 1–10.
Sanderson, D., Marchini, R.D., 1984. Transpression. J. Struct. Geol. 6, 449–458.
Santos, L.C.M.d.L., Dantas, E.L., Santos, E.J.d., Santos, R.V., Lima, H.M., 2015. Early to late Paleoproterozoic magmatism in NE Brazil: the Alto Moxotó terrane and its tectonic implications for the pre-West Gondwana assembly. J. S. Am. Earth Sci. 58, 188–209.
Santos, L.C.M.d.L., Dantas, E.L., Vidotti, R.M., Cawood, P.A., dos Santos, E.J., Fuck, R.A., Lima, H.M., 2017. Two-stage terrane assembly in Western Gondwana: insights from structural geology and geophysical data of central Borborema Province, NE Brazil. J. Struct. Geol. 103, 167–184. https://doi.org/10.1016/j.jsg.2017.09.012.
Santos, L.C., de Oliveira, R., Lages, de A., Dantas, G.L., E., Caxito, F., Cawood, P.A., Fuck, A., Lima, R.M., Santos, H.L., G., de Araújo Neto, J.F., 2021. Evidence for Neoproterozoic terrane accretion in the central Borborema Province, West Gondwana deduced by isotopic and geophysical data compilation. Int. Geol. Rev. 1–20.
Silva, V.L., Neves, S.P., 2021. Transition from contractional to transpressive tectonics: evidence from the Feira Nova region, Rio Capibaribe domain, Borborema province, NE Brazil. Braz. J. Geol. 51, 12. https://doi.org/10.1590/2317-4889202120200049.
Simpson, C., 1983. Displacement and strain patterns from naturally occurring shear zone terminations. J. Struct. Geol. 5, 497–506.
Simpson, C., De Paor, D.G., 1993. Strain and kinematic analysis in general shear zones. J. Struct. Geol. 15, 1–20.
Souza, Z.S., Montel, J.-M., Gioia, S.M.L.C., Maia de Hollanda, M.H.B., Leite do Nascimento, M.A., Jardim de Sá, E.F., Amaro, V.E., Pimentel, M.M., Lardeaux, J.-M.,

Veschambre, M., 2006. Electron microprobe dating of monazite from high-T shear zones in the São José de Campestre Massif, NE Brazil. Gondwana Res. 9, 441–455.
Spector, A., Grant, F.S., 1970. Statistical models for interpreting aeromagnetic data. Geophysics 35, 293–302.
Stewart, J.R., Betts, P.G., 2010. Late Paleo-Mesoproterozoic plate margin deformation in the southern Gawler Craton: insights from structural and aeromagnetic analysis. Precambrian Res. 177, 55–72.
Tikoff, B., Teyssier, C., 1994. Strain modeling of displacement-field partitioning in transpressional orogens. J. Struct. Geol. 16, 1575–1588.
Tommasi, A., Vauchez, A., Daudré, B., 1995. Initiation and propagation of shear zones in a heterogeneous continental lithosphere. J. Geophys. Res. Solid Earth 100, 22083–22101.
Trindade, R.I.F., Raposo, M.I.B., Ernesto, M., Siqueira, R., 1999. Magnetic susceptibility and partial anhysteretic remanence anisotropies in the magnetite-bearing granite pluton of Tourao, NE Brazil. Tectonophysics 314, 443–468.
Van Schmus, W.R., Oliveira, E.P., Silva Filho, A.F., Toteu, S.F., Penaye, J., Guimarães, I. P., 2008. Proterozoic links between the Borborema province, NE Brazil, and the central African fold belt. From. In: Pankhurst, R.J., Trouw, R.A.J., Brito Neves, B.B., De Wit, M.J. (Eds.), West Gondwama: Pre-cenozoic Correlations across the South Atlantic Region, vol. 294. Geological Society of London, Special Publications, pp. 69–99. https://doi.org/10.1144/SP294.5.
Van Schmus, W.R., Kozuch, M., de Brito Neves, B.B., 2011. Precambrian history of the Zona transversal of the Borborema province, NE Brazil: insights from Sm-Nd and U-Pb geochronology. J. S. Am. Earth Sci. 31, 227–252.
Vasconcelos, D.L., Bezerra, F.H.R., Medeiros, W.E., de Castro, D.L., Clausen, O.R., Vital, H., Oliveira, R.G., 2019. Basement fabric controls rift nucleation and postrift basin inversion in the continental margin of NE Brazil. Tectonophysics 751, 23–40.
Vauchez, A., Egydio-Silva, M., 1992. Termination of a continental-scale strike-slip fault in partially melted crust: the West Pernambuco shear zone, northeast Brazil. Geology 20, 1007–1010.
Vauchez, A., Neves, S.P., Caby, R., Corsini, M., Egydio-Silva, M., Arthaud, M., Amaro, V., 1995. The Borborema shear zone system, NE Brazil. J. S. Am. Earth Sci. 8, 247–266.
Vauchez, A., Tommasi, A., Barruol, G., 1998. Rheological heterogeneity, mechanical anisotropy and deformation of the continental lithosphere. Tectonophysics 296, 61–86.
Viegas, L.G.F., Archanjo, C.J., Hollanda, M.H.B.M., Vauchez, A., 2014. Microfabrics and zircon U–Pb (SHRIMP) chronology of mylonites from the Patos shear zone (Borborema Province, NE Brazil). Precambrian Res. 243, 1–17.
Vos, I.M.A., Bierlein, F.P., Barlow, M.A., Betts, P.G., 2006. Resolving the nature and geometry of major fault systems from geophysical and structural analysis: the Palmerville Fault in NE Queensland, Australia. J. Struct. Geol. 28, 2097–2108.
Walsh, J.J., Bailey, W.R., Childs, C., Nicol, A., Bonson, C.G., 2003. Formation of segmented normal faults: a 3-D perspective. J. Struct. Geol. 25, 1251–1262.
Wijns, C., Perez, C., Kowalczyk, P., 2005. Theta map: edge detection in magnetic data. Geophysics 70, L39–L43. https://doi.org/10.1190/1.1988184.
Xypolias, P., 2010. Vorticity analysis in shear zones: a review of methods and applications. J. Struct. Geol. 32, 2072–2092.
Xypolias, P., Spanos, D., Chatzaras, V., Kokkalas, S., Koukouvelas, I., 2010. Vorticity of flow in ductile thrust zones: examples from the Attico-Cycladic Massif (Internal Hellenides, Greece). Geol. Soc., Lond., Spl. Publ. 335, 687–714. https://doi.org/10.1144/sp335.28.

SUPPLEMENTARY MATERIAL

The Patos-Pernambuco shear system of NE Brazil: partitioned intracontinental transcurrent deformation revealed by enhanced aeromagnetic data

Haakon Fossen [a,*], Lyal B. Harris[b], Carolina Cavalcante[c], Carlos José Archanjo[d], Carlos F. Ávila[d]

[a] Museum of Natural History/Department of Earth Science, University of Bergen, Allégaten 41, 5007 Bergen, Norway

[b] INRS-ETE, 490 de la Couronne, Québec (QC), G1K 9A9 Canada

[c] Departamento de Geologia, Universidade Federal do Paraná, Av. Cel. Francisco Heráclito dos Santos, 100, Centro Politécnico, Curitiba (PR), 81531-980, Brazil

[d] Instituto de Geociências, Universidade de São Paulo, São Paulo (SP), Brazil

This section includes both larger, high resolution copies of some images in the main article as well as some additional, complementary figures which, for space reasons, could not be included in the article.

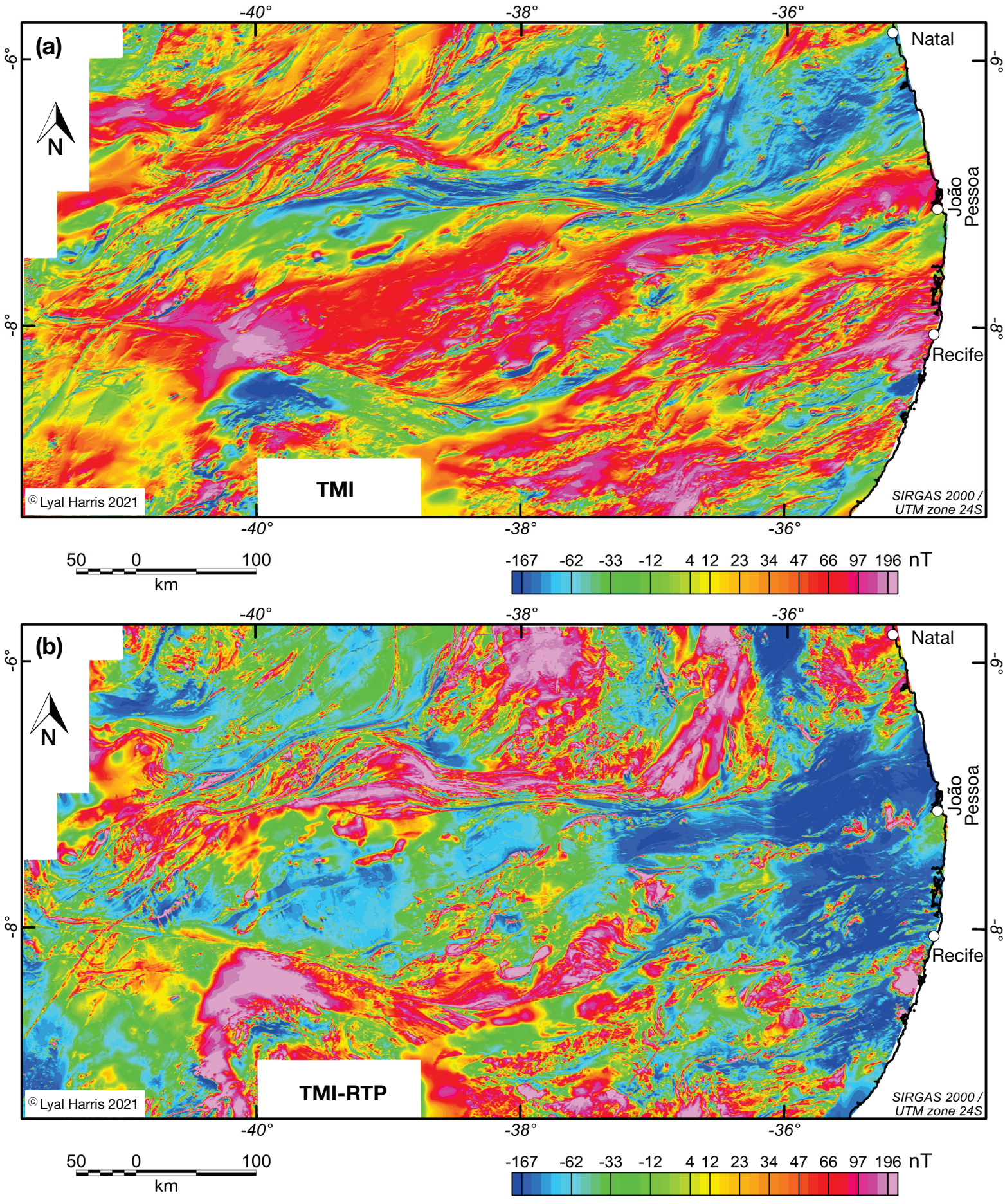

Figure SM1. Comparison between original data and data reduced to the pole (the colour scale is the same in both). (a) Original CPRM aeromagnetic data (TMI), (b) Aeromagnetic data reduced to the pole (TMI-RTP).

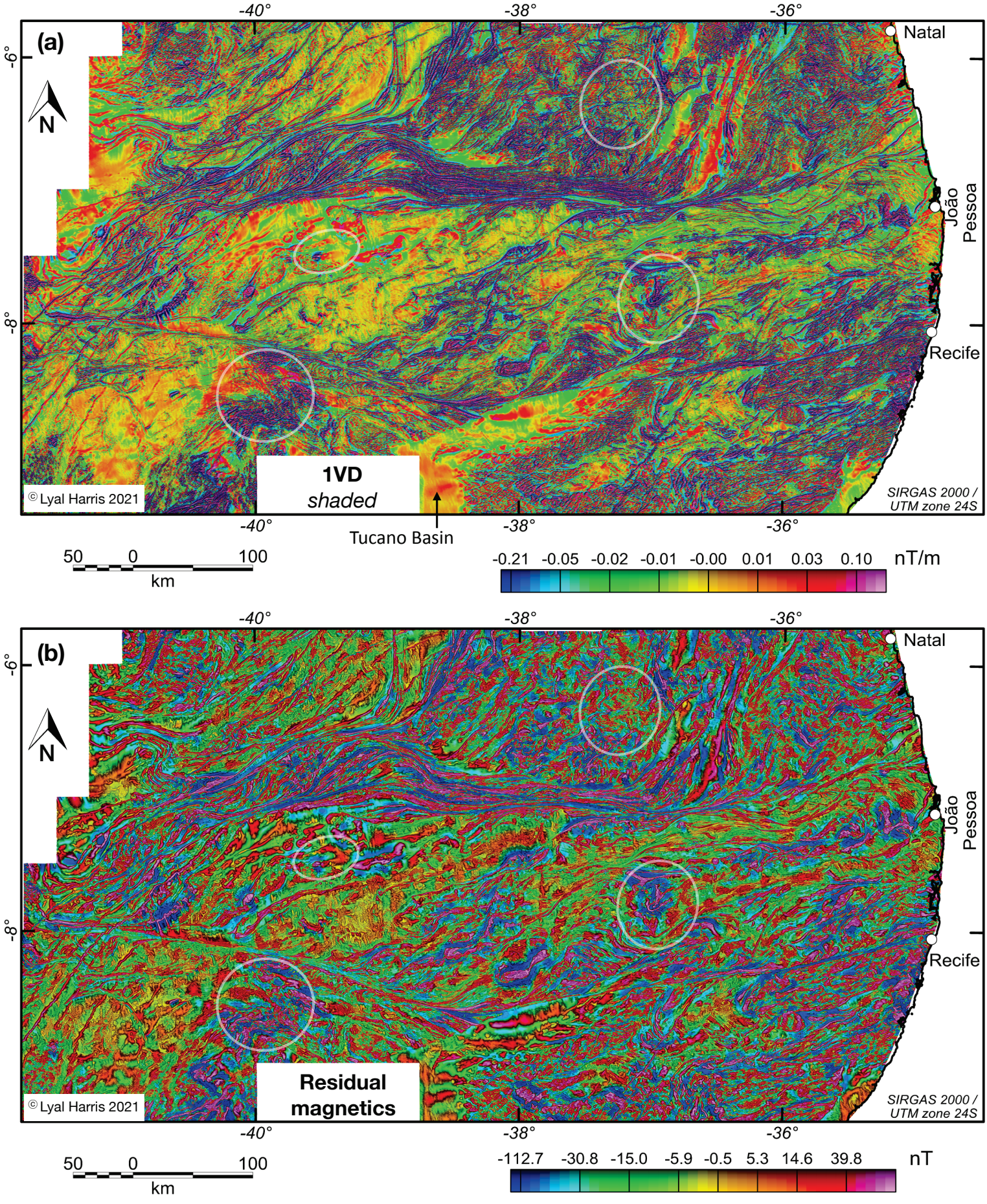

Figure SM2. Comparison between shaded first vertical derivative (1VD) of data reduced to the pole conventionally used in (a) and the shaded residual component extracted through power spectrum based filtering (b). Both treatments enhance near surface features, however structures are sharper and more readily discernable in (b). For example, folds highlighted by transparent white ellipses in (b) cannot be seen, or are less apparent in (a).

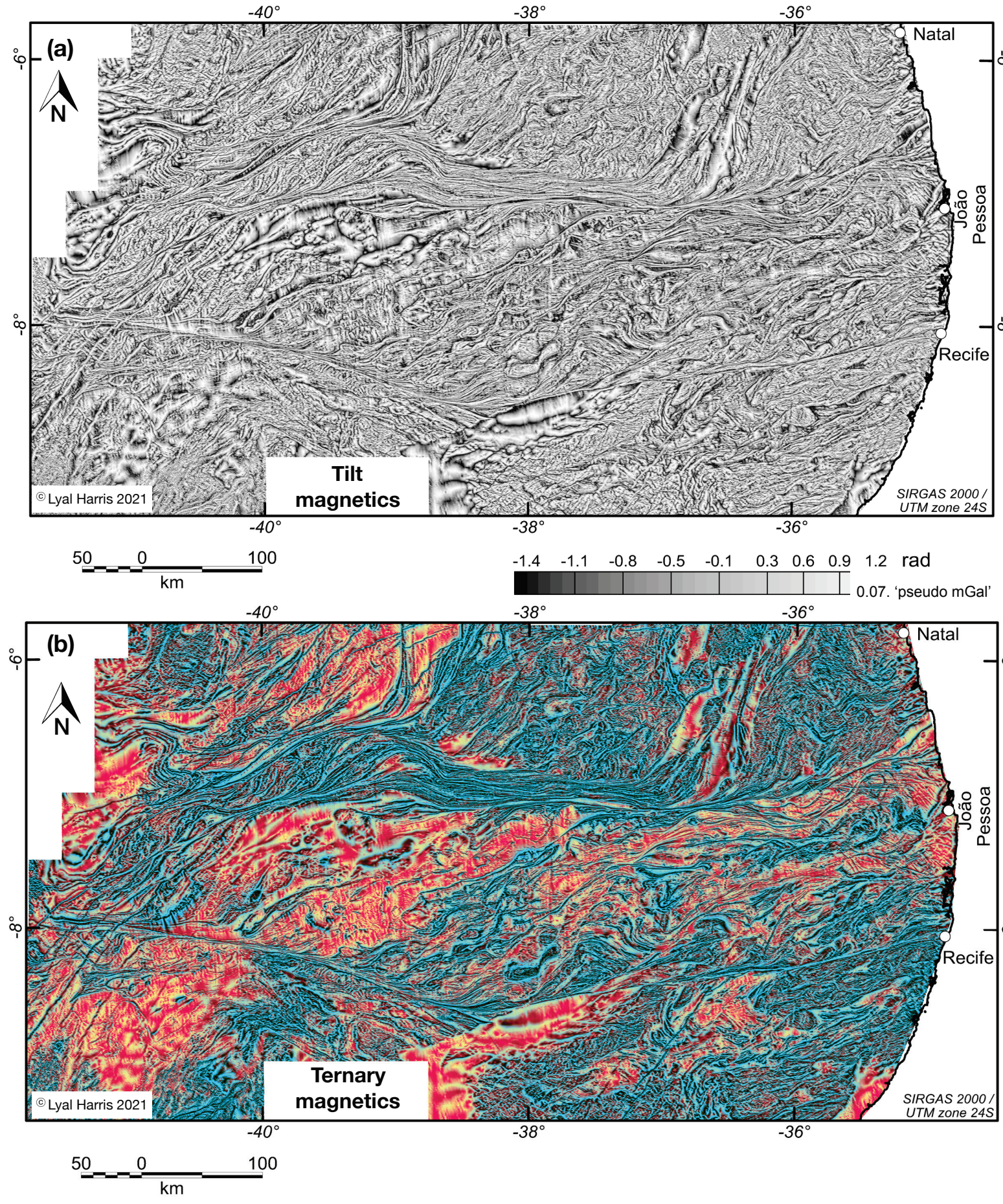

Figure SM3. Enhancements of residual aeromagnetic data which enhance geological structures, contacts and intrusions. (a) Tilt angle. (b) Ternary gradients.

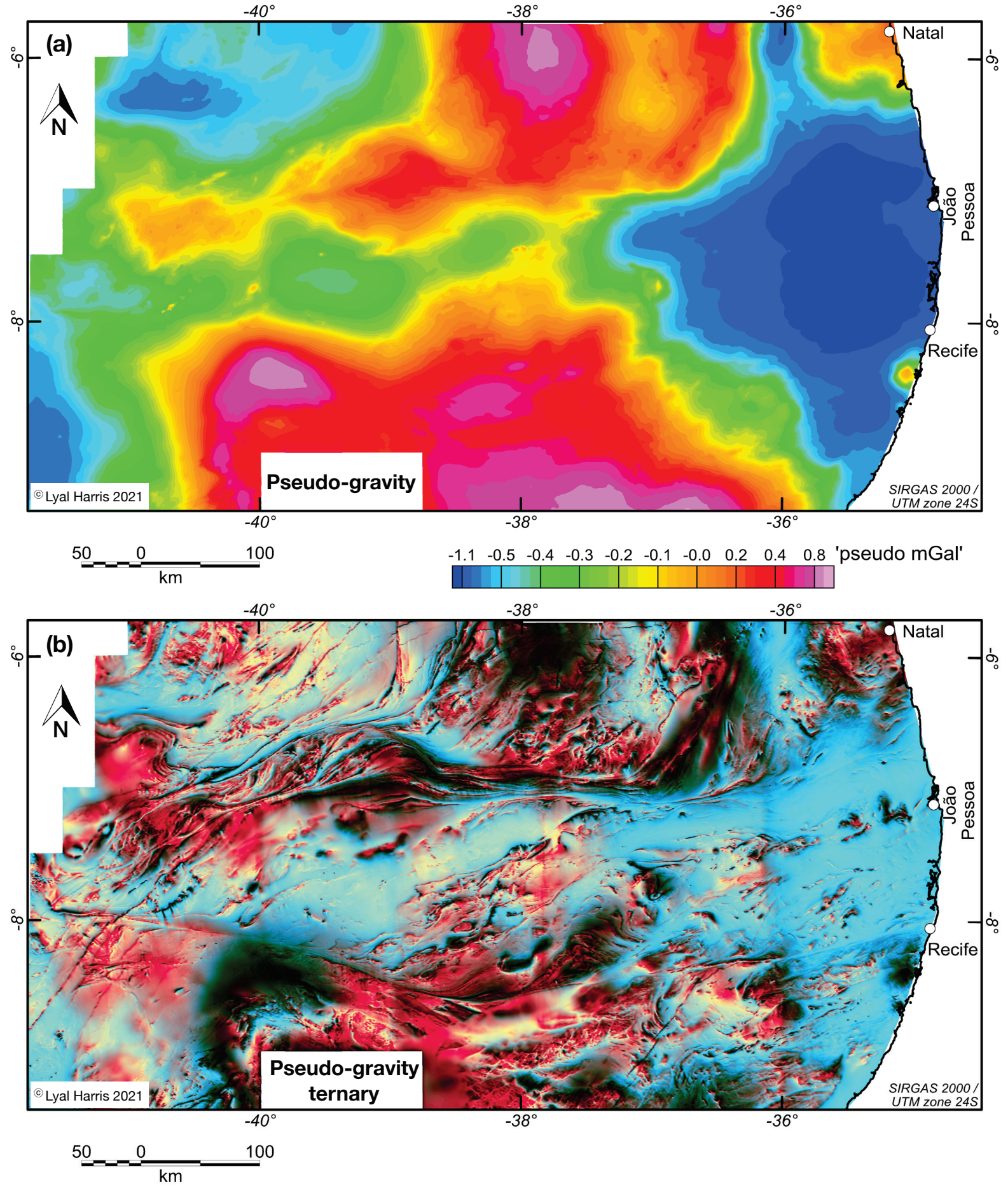

Figure SM4. Pseudo-gravity derived from aeromagnetic data (see main article and Harris, this volume, for explanations). The total field pseudo-gravity image in (a) is dominated by its long wavelength component highlighting deep crustal domains. The ternary gradient image in (b) highlights different litho-stratigraphic units and intrusions, providing complementary data to the TMI-RTP image in Figure SM1b.

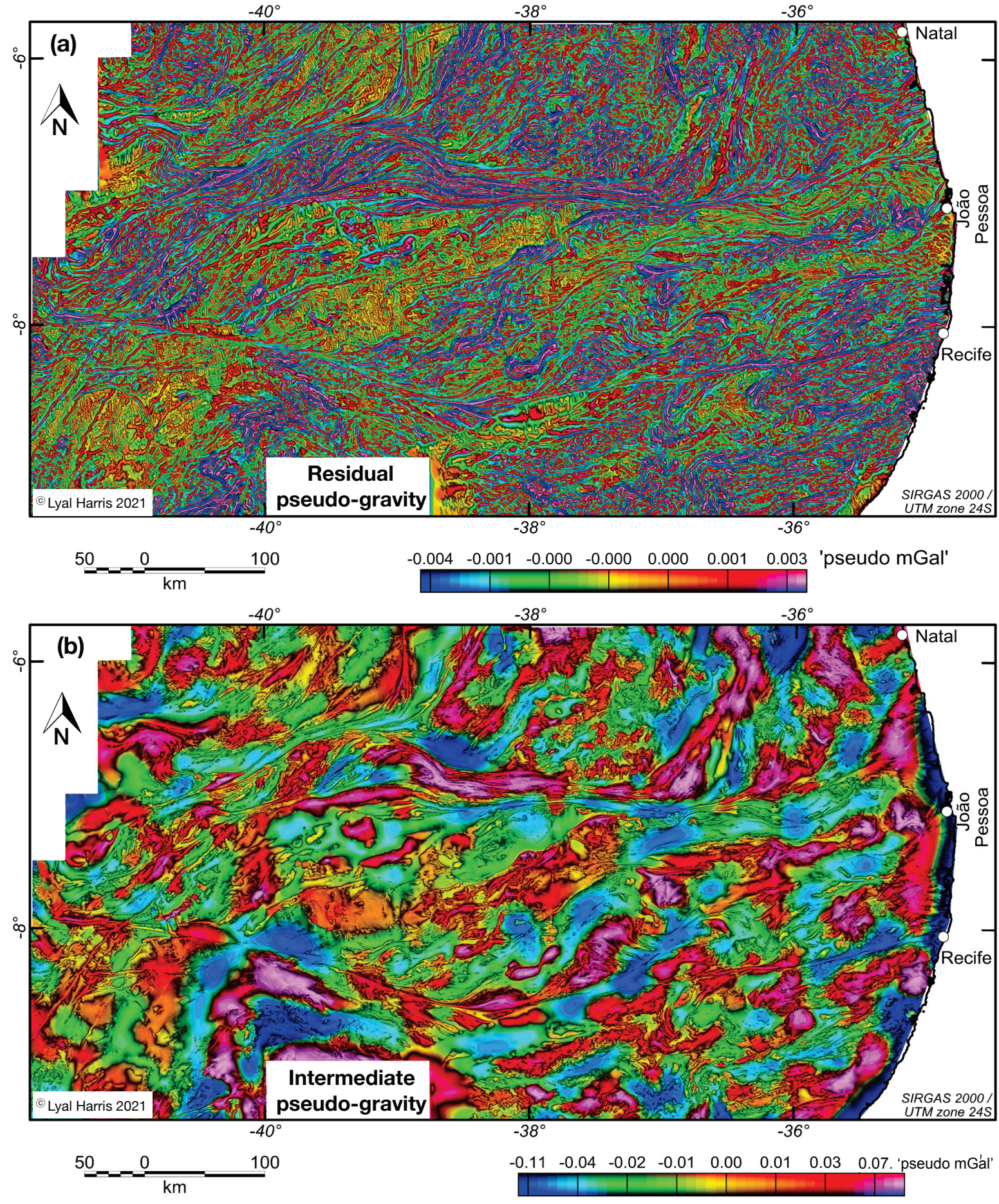

Figure SM5 *(legend on following page)*

Figure SM5 *(previous page).* Upper (a) and middle (b) crustal pseudo-gravity components. The residual pseudo-gravity image in (a), whilst greatly resembling the residual aeromagnetic image in Figure SM2b, on close inspection shows more details of fine layering and their folding and offset along shear zones, highlighting the presence of more sinistral antithetic shear zones than seen in the residual aeromagnetic image. An intermediate wavelength depth slice through the mid-crust in (b) is extremely useful in tracing different litho-stratigraphic packages from the Northern and Southern domains into the Central Domain to establish the amount of dextral displacement across this shear system.

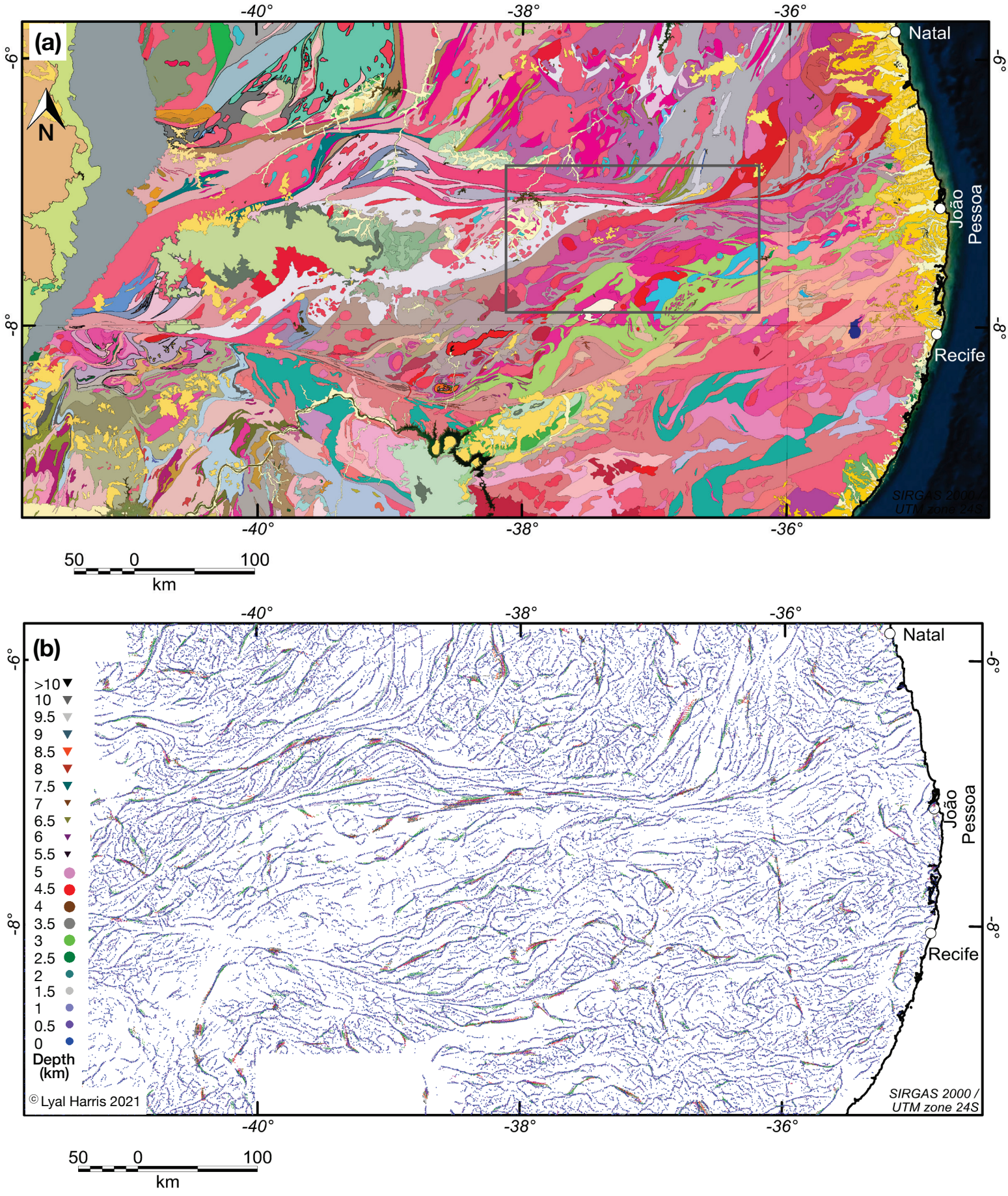

Figure SM6 *(continues on following page)*

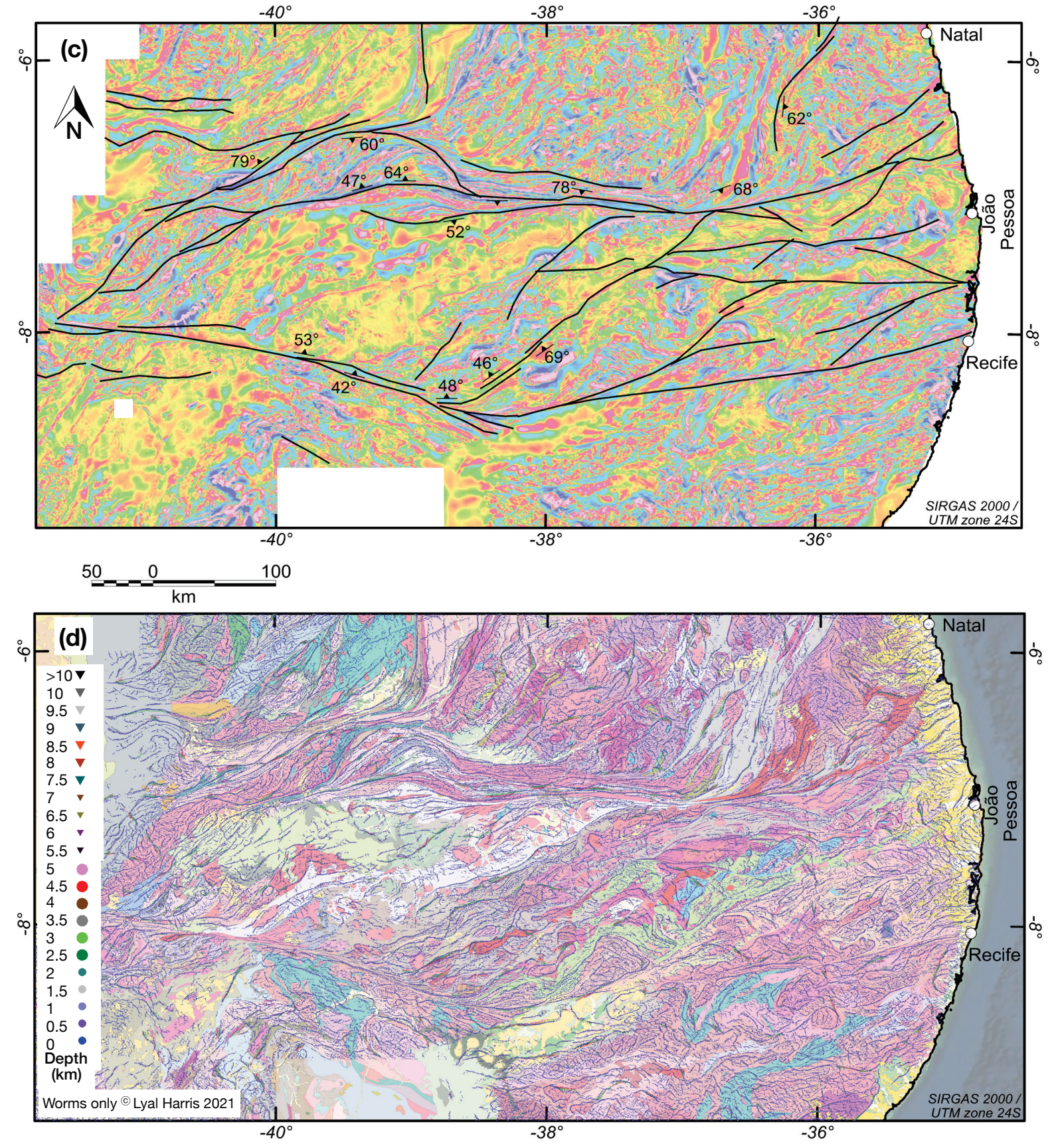

Figure SM6. (a) Litho-stratigraphic map of the study area from the Brazilian Geological Survey, CPRM. The legend for the enlarged area (rectangle) follows Figure SM7(c). For the full map legend, consult the original online GIS version on https://geoportal.cprm.gov.br/geosgb/. (b) Pseudogravity worms. (c) Representative dips calculated from pseudogravity worms and a simplified shear zone map. The shallow dips on the NE-SW shear with sinistral horizontal offsets suggests a likely thrust component due to its orientation. (d) Pseudogravity worms overlain on the geology map in (a).

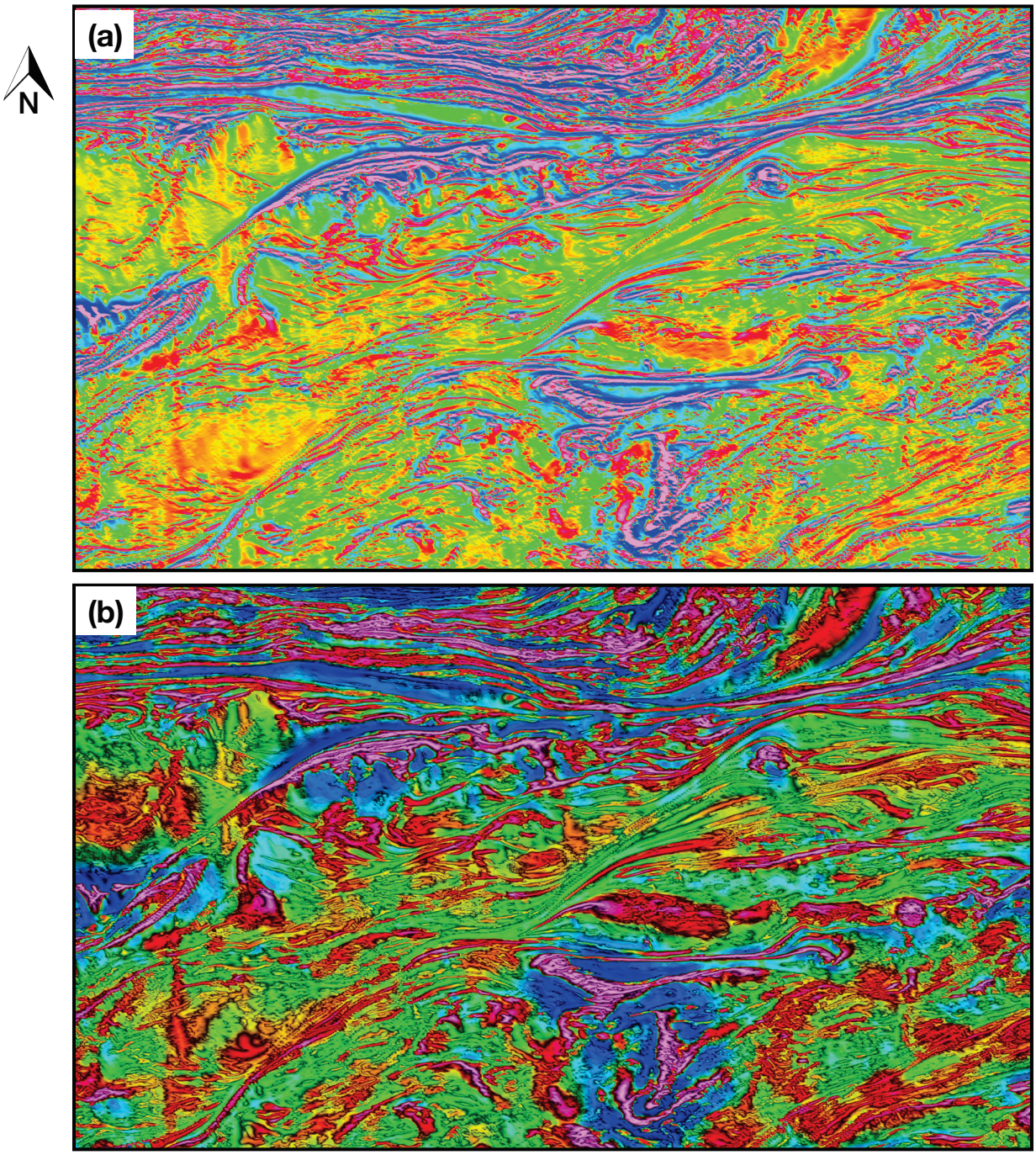

Figure SM7 *(continues on following page)*

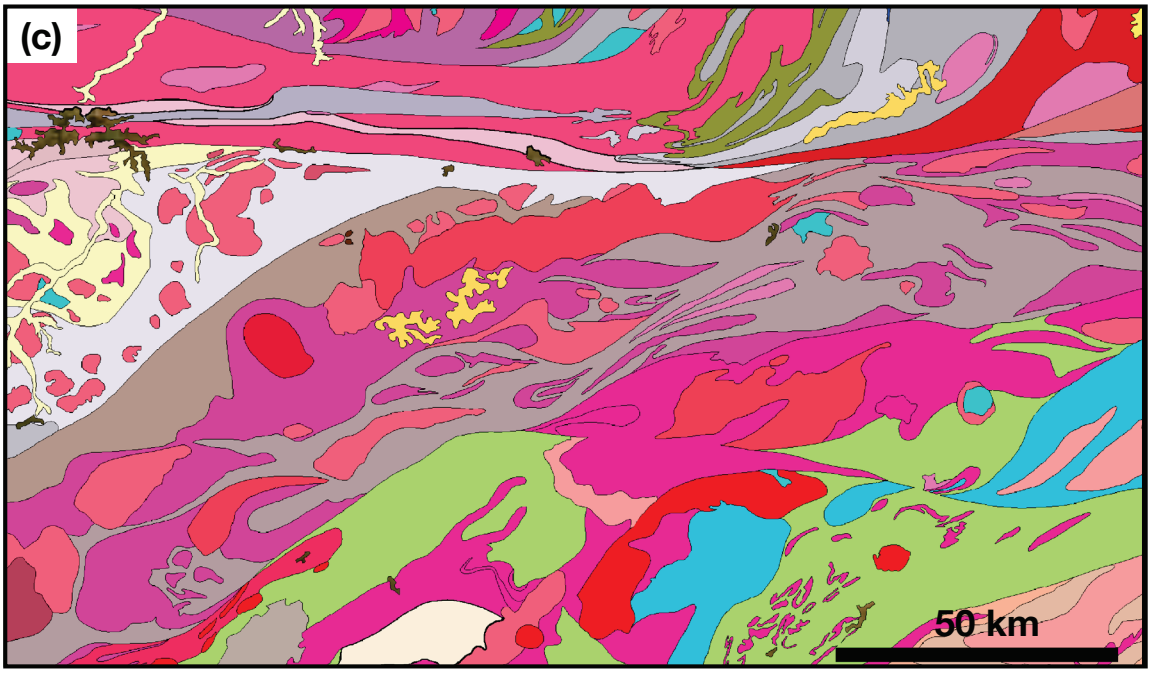

Phanerozoic

- Alluvium, laterite, etc.

Neoproterozoic

- Alkali feldspar granite, syenite
- Diorite, gabro, gabronorite, granodiorite, tonalite
- Meta-conglomerate, muscovite quartzite
- Quartz-biotite±garnet schist, quartzite, meta-volcanics
- BIF, meta-conglomerate, meta-graywacke, meta-volcanics
- Chlorite & tremolite chlorite schist, BIF, meta-ultramafic & basalt
- Calcsilicates, chert, metavolcanics, meta-tuffs
- Orthogneiss
- Orthogneiss & migmatite

Mesoproterozoic

- Metasedimentary & metavolcanic rocks

Palaeoproterozoic

- Amphibolite, ortho- & paragneiss
- Leuco-orthogneiss, paragneiss, migmatite, meta-gabbro
- Sillimanite, muscovite, biotite gneiss, migmatites, mylonites to ultramylonites
- Augen gneiss, migmatite
- Hornblende gneiss
- Meta-granite, migmatite

Figure SM7 *(continues on following page)*

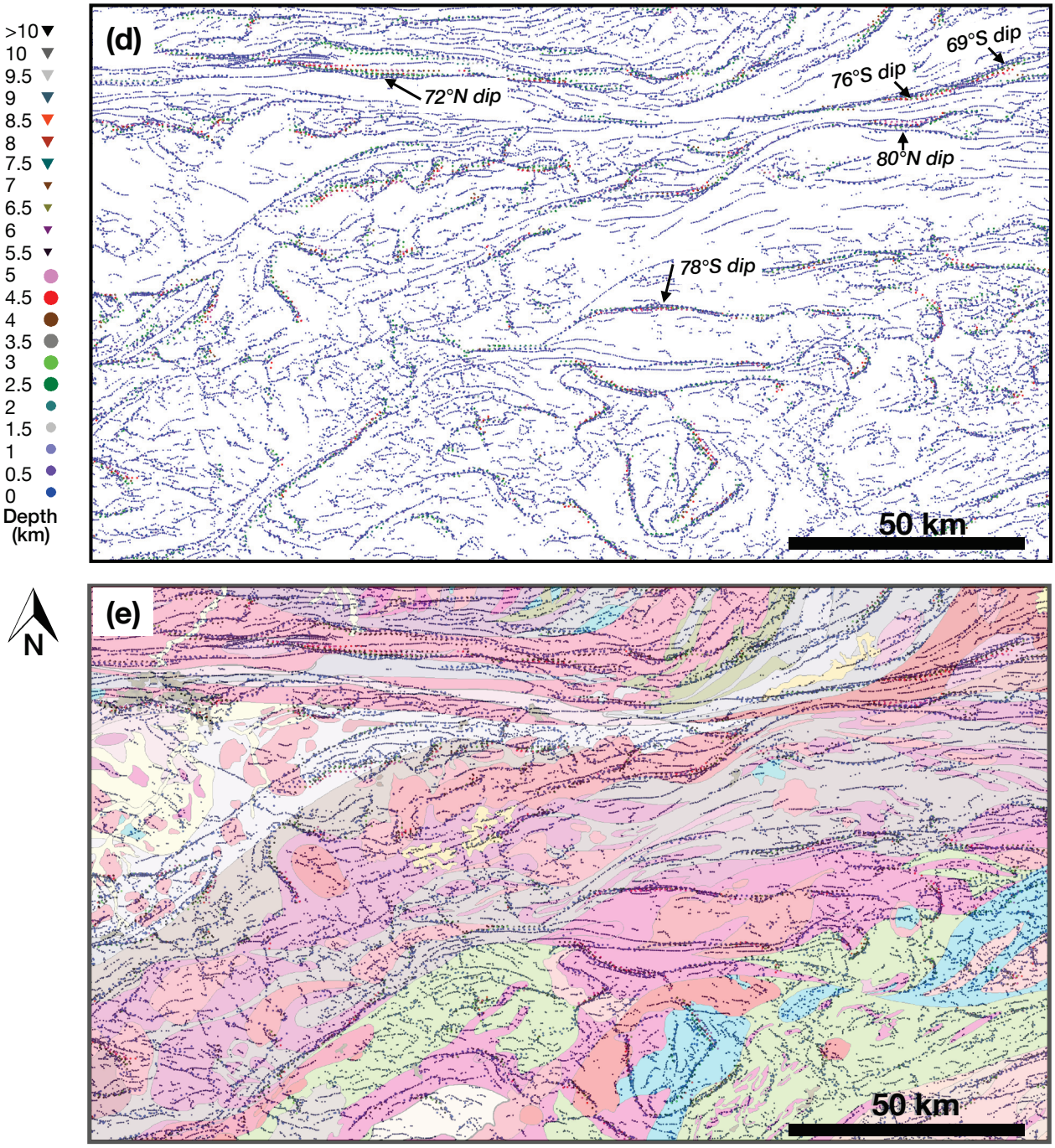

Figure SM7. Comparison of different data for an enlargement of the area shown in Figure SM6(a). (a) 1VD. (b) Shaded residual. (c) CPRM geological map and legend to main lithologies. For the full map legend, consult the original online GIS version on https://geoportal.cprm.gov.br/geosgb/. (d) Worms illustrating how dips may be calculated through measuring the horizontal offset of worms at known depths (here between the surface and 5 km). (e) Relationship between worms and mapped geology.

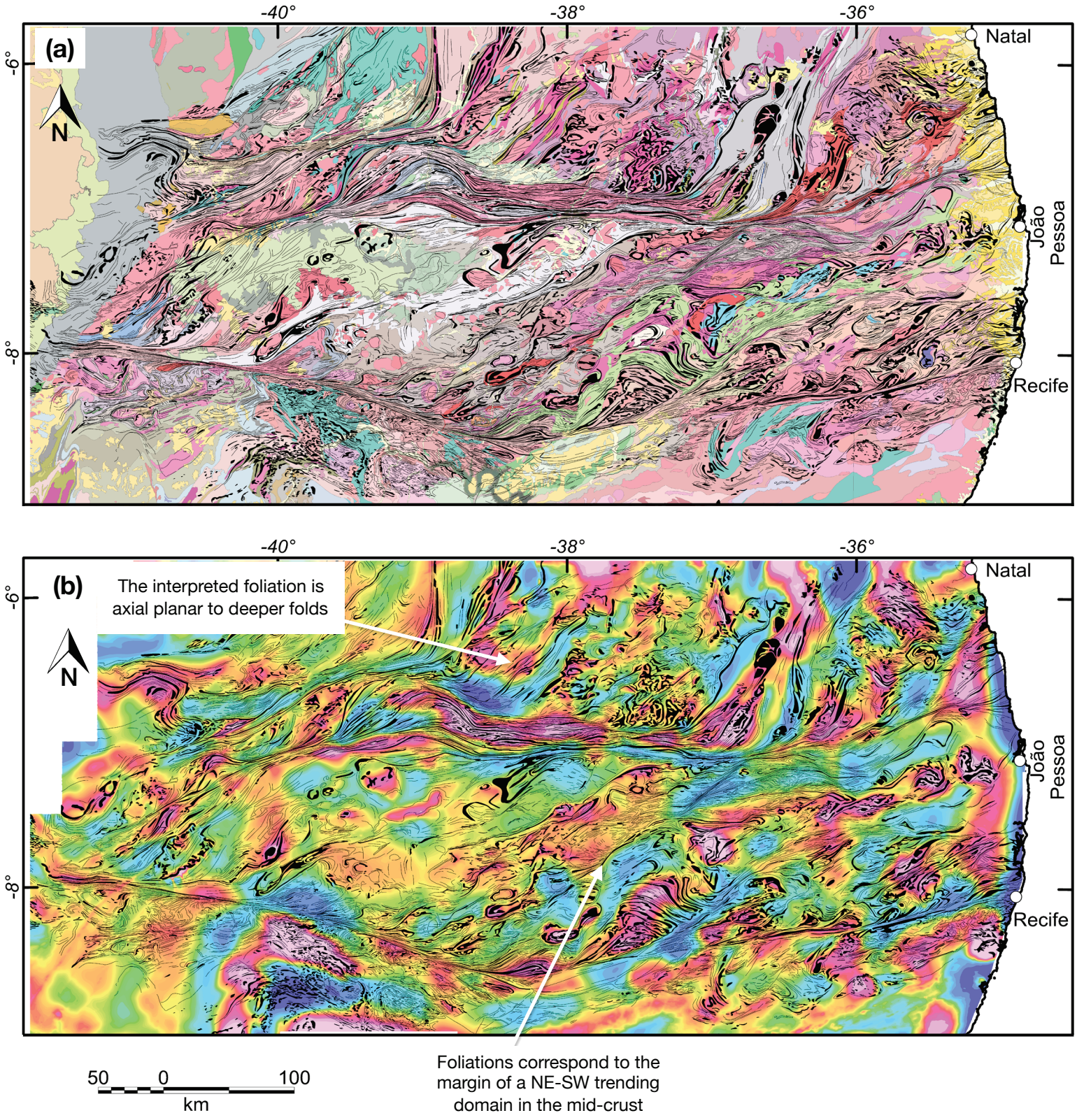

Figure SM8. Manually drawn foliation trajectory superposed on: (a) CPRM geological map. The foliation trajectory traced from enhanced residual aeromagnetics images shows an excellent correlation with mapped geological contacts. (b) Intermediate wavelength pseudo-gravity image highlighting deeper structures.

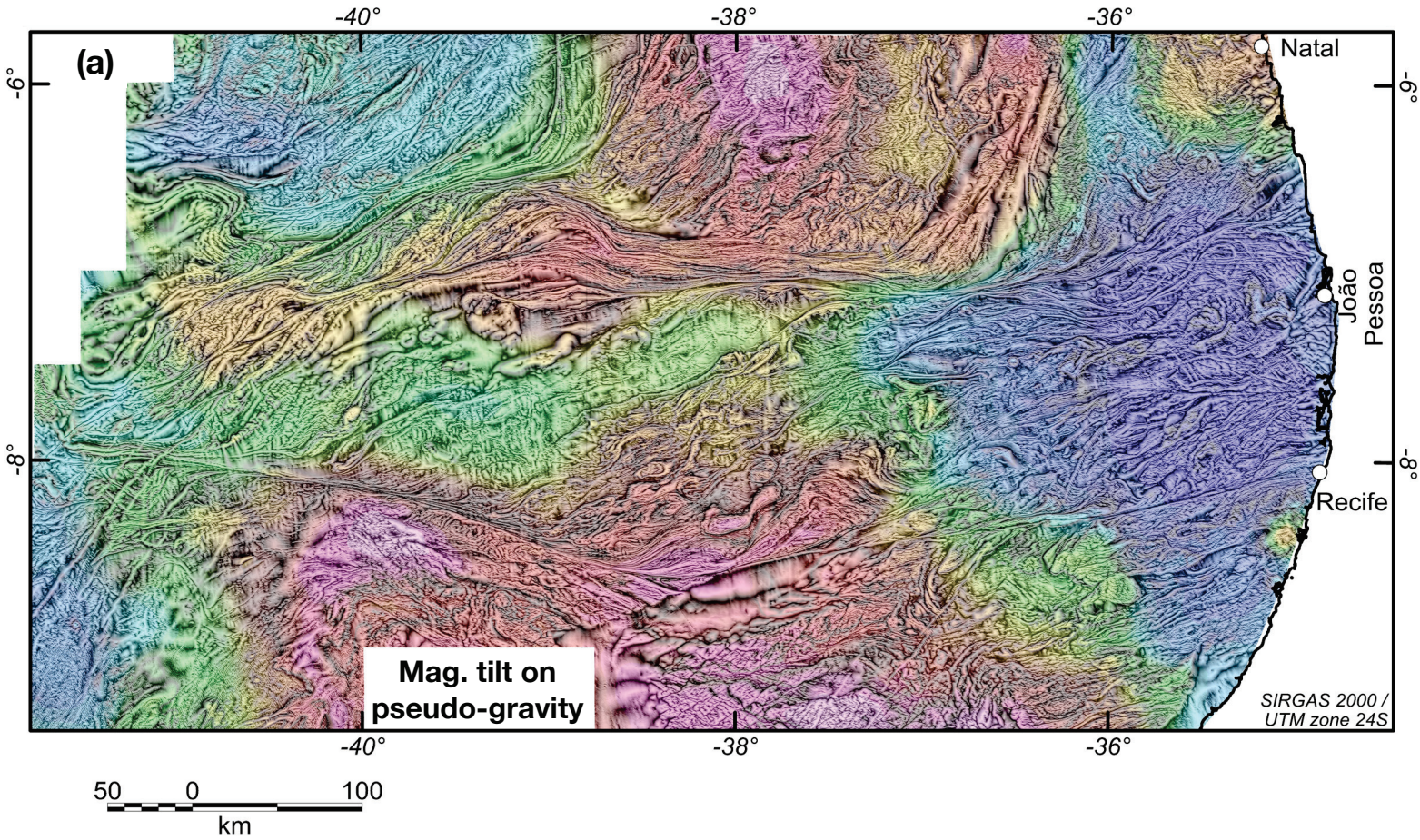

Figure SM9. Residual magnetic tilt image in gray overlain on total field pseudo-gravity to show the relationship between upper and deep crustal domains.

Figure S_LH9.